

Cristian Făciu · Alain Molinari

The structure of shock and interphase layers for a heat conducting Maxwellian rate-type approach to solid–solid phase transitions

Part II: numerical study for an SMA model

Received: 14 October 2012 / Revised: 20 January 2013
© Springer-Verlag Wien 2013

Abstract One continues the qualitative analysis started in Part I (Făciu and Molinari in Acta Mech) concerning the thermomechanical characteristics of a steady, structured moving phase boundary in a shape memory alloy (SMA) by a quantitative investigation. The internal structure of these interphase layers is governed by a Maxwellian rate-type constitutive equation coupled or not with the Fourier heat conduction law. We consider as equilibrium stress–strain–temperature response function for the Maxwellian model an explicit piecewise linear thermoelastic relation for an SMA bar which can exist in the austenite phase A and in two variants of martensite M^\pm . Its thermal properties are built in agreement with experimental results on NiTi. This equilibrium relation has the atypical property that not only the derivative of the stress response function with respect to the strain changes its sign, but also the derivative with respect to the temperature. Considerable temperature variation is generated by impact-induced phase transformations due to the large amount of latent heat released (absorbed) inside the transition layer. One gets strong heating (cooling) across a compressive $A \rightarrow M^-$ (expansive $M^- \rightarrow A$) propagating interphase layer. A significant lower (larger) temperature than that at the front and Hugoniot back state is obtained inside an impact-induced $M^+ \rightarrow M^-$ ($M^- \rightarrow M^+$) interphase layer. The experimental finding of this phenomenon of temperature undershoot (overshoot) could be a valuable indication for the existence of an interphase layer.

1 Introduction

While the discontinuous shock wave theory in condensed matter is extremely useful in many applications involving impact loading conditions, the use of shock layer theory, characterized by a small interval of rapid transition induced by viscosity, heat conduction, or other structuring parameter, can have important theoretical and experimental consequences. For example, steady plastic shock waves have been observed in the 1960s, but their definitive experimental evidence is due to Barker [2] who, by using a new technique of laser velocity interferometry, has brought an important contribution to the development of constitutive theory of viscoplastic materials by the discovery of the “fourth power law.” About this law and the role of viscosity in the structuring of shock waves in metals, an overview can be found in Molinari and Ravichandran [3] and Grady [4].

Steady-propagating plastic shock waves have been analyzed from plate-impact experiments by measuring the rear surface velocity history at the free surface of the target specimen using laser interferometry. Propagating

C. Făciu (✉)
“Simion Stoilow” Institute of Mathematics of the Romanian Academy, Research Unit No. 6,
P.O. Box 1-764, 014700 Bucharest, Romania
E-mail: Cristian.Faciu@imar.ro

A. Molinari
Laboratoire d’Etude des Microstructures et de Mécanique des Matériaux, UMR-CNRS 7239,
Labex Damas, Université de Lorraine, Ile du Saulcy, 57045 Metz, France
E-mail: Molinari@lpm.univ-metz.fr

phase boundaries cannot be directly observed by this method. That is due to their low propagation speed with respect to the sound speed and to the wave interactions and reflections following the impact which hinders the generated phase boundary to reach the monitoring surface. The presence of a propagating phase boundary and its speed can be deduced only in an indirect way from measurements of the elastic waves at the rear end of the target specimen (see Escobar and Clifton [5] and the theoretical study [6]).

Other experiments in which a flyer plate or projectile strikes a target specimen and induces a propagating phase boundary have been also carried out. Shock-induced graphite-to-diamond martensitic phase transitions are described in Erskine and Nellis [7], while in SMAs, they have been investigated for instance by Lagoudas et al. [8], Niemczura and Ravi-Chandar [9]. These dynamic experiments use different methods to identify mechanical characteristics of the transformation front, but neglect the large temperature variation generated after the passage of the wave front which can be an extremely valuable manifestation of a phase transforming process. That is obviously due to the fact that such measurements require adequate temperature diagnostic tools to record short-lived transient phenomena.

The incorporation of thermal effects into the continuum modeling of impact-induced solid–solid phase transitions has been considered, for example, by Abeyaratne and Knowles [10–12] in the framework of a driving force theory, by Chen and Lagoudas [13, 14] and Lagoudas et al. [8] using a theory based on a volume fraction as internal variable. Solutions with *sharp discontinuities* have been obtained for the corresponding impact problems. Another way to model the response of phase transforming materials is to introduce an internal dissipation by augmenting the thermoelastic law in such a way that the stress depends additionally on strain-rate (the Kelvin–Voigt approach used in Vainchtein [15, 16]) and on spatial strain-gradients (the “viscosity-capillarity” model used in Slemrod [17], Abeyaratne and Knowles [18], Turteltaub [19], Ngan and Truskinovsky [20, 21]), or the so-called Maxwellian rate-type approach for which the stress depends additionally on strain-rate and stress-rate used in Făciu and Mihăilescu-Suliciu [22], Făciu and Molinari [6] and in Part I [1]. These augmented theories replace the sharp discontinuities by *transition layers of finite thickness*.

The Maxwellian model, which we consider in the following, includes as a limit case the Kelvin–Voigt model. It introduces a *time of relaxation* related to a “viscosity” parameter in the Maxwellian rate-type relation which characterizes the kinetics of phase transition. Indeed, in quasi-static loading conditions, this rate-type approach allows to capture automatically the material instability phenomena which lead to the nucleation and growth of phases in the unstable regions without additional nucleation criterion (see Făciu and Mihăilescu-Suliciu [22]). Thus, the transition process of a particle from one stable phase to another does not occur instantaneously, but it requires a finite phase transition time. The rate of growth of the instability is inverse proportional with this time of relaxation (see Făciu and Molinari [6]). In the case of dynamic loading conditions, the time of relaxation is a structuring parameter for a moving interphase layer. Another structuring parameter is the heat conduction which even alone has the capacity to structure shock waves as it was shown in the comprehensive study on thermoelastic materials by Dunn and Fosdick [23].

In the first part [1], we have developed a detailed treatment of steady, structured shock waves in a general framework for a thermoelastic SMA bar. The newness of this study consists in the fact that the internal structure of these traveling waves is governed by a constitutive approach which has not been considered until now, namely the Maxwellian rate-type constitutive equation coupled or not with the Fourier heat conduction law. Moreover, we have considered a thermoelastic stress–strain–temperature relation $\sigma = \sigma_{eq}(\varepsilon, \theta)$ with the properties that both derivatives $\frac{\partial \sigma_{eq}}{\partial \varepsilon}$ and $\frac{\partial \sigma_{eq}}{\partial \theta}$ change their sign in the constitutive domain. The first property is usual for a phase transforming material, but the second one is atypical for thermoelastic materials, and its outcomes have not been investigated systematically until now. This second property is based on laboratory experiments and expresses the fact that in traction tests, the stress plateaus of the hysteresis loop increase, while in compression tests, the stress plateaus of the hysteresis loop decrease as the temperature grows. In addition, this property has important consequences on thermal features of the internal structure of the interphase layers which could be exploited from experimental point of view.

The aim of this paper is to complete this qualitative analysis with a quantitative description. To do this, we introduce in Sect. 2 an explicit piecewise linear thermoelastic model $\sigma = \sigma_{eq}(\varepsilon, \theta)$ with non-monotone stress–strain relation for a certain range of temperature θ . This model is appropriate to characterize phenomenological aspects of the thermomechanical response of an SMA bar in tension and compression tests. It corresponds to a material capable of existing in three distinct solid phases: the austenite A and two variants of martensite M^\pm . The numerical parameters of the proposed thermoelastic model are chosen in such a way that the evolution of the non-monotone stress–strain relation with the temperature is quantitatively consistent with the rate of increase of the hysteresis plateau with temperature obtained by Shaw [24] in traction tests for NiTi strips in the

range of temperatures between 15 and 55 °C. In this approach, the free energy of the thermoelastic model is not prescribed a priori, but on the contrary is determined once the stress–strain–temperature relation has been established. The thermodynamic potentials of the thermoelastic model are characterized in Appendix A. We also introduce in Sect. 2 the mixed hyperbolic–elliptic system of field equations and the jump relations for the three-phase thermoelastic material. The internal energy allows us to explicitly determine the Hugoniot locus in the temperature–strain space and in the stress–strain space. In Sect. 3, we use this thermoelastic model as an equilibrium relation for a Maxwellian rate-type constitutive equation. The thermodynamic potentials of the Maxwellian model are explicitly determined for this equilibrium relation in Appendix B. The procedure for finding traveling wave solutions structured by rate-type effects (“viscosity”) and heat conduction is outlined in Sect. 4. In Sect. 5, we describe the prediction of our constitutive approach for impact-induced phase transformations from the austenite phase A to the martensitic variant M^- and for the reverse situation. In this case, $\frac{\partial \sigma_{eq}}{\partial \theta}$ has a constant negative sign inside the profile layer. We illustrate how after the passage of the moving interface separating the two phases of the material the temperature increases in the compressive case and decreases in the expansive case. The considerable increase or decrease in temperature is due to the large amount of latent heat released or absorbed during the phase transformation inside the transition layer. We also consider the case of an impact-induced compressive phase transformation from the martensite variant M^+ to the martensite variant M^- when $\frac{\partial \sigma_{eq}}{\partial \theta}$ changes its sign inside the interphase layer. This is the most interesting case through its theoretical and practical consequences. Indeed, in this case, the material is heated by the passage of the compressive moving phase boundary, i.e., the temperature of the Hugoniot back state is significantly higher than the temperature of the front state, but there are places inside the transition layer where the temperature is considerably lower than the front and back state temperature. This phenomenon of temperature undershoot in a steady structured wave is in agreement with the endothermic character of the $M^- \rightarrow A$ transformation and the exothermic character of the $A \rightarrow M^+$ transformation. This behavior cannot be predicted by a sharp interface theory where only the front state and the admissible Hugoniot back state are relevant. On the other side, the existence of this spike-layer form of the temperature profile gives the possibility to an interphase layer to be detected experimentally. Finally, Sect. 6 contains conclusions and discussions.

2 A piecewise linear thermoelastic model for a three-phase SMA

It is now unanimously accepted that the main features of solid–solid phase transitions, like in shape memory alloys, are predicted by using thermoelastic constitutive laws with non-monotone stress–strain relations for certain intervals of temperature. We consider here an explicit and simple relation $\sigma = \sigma_{eq}(\varepsilon, \theta)$, called equilibrium stress–strain–temperature relation, which fulfills the thermomechanical assumptions **H1–H3** described in Part I [1]. It characterizes the response of an SMA bar which can exist in three phases: the (low strain) austenite phase A and two variants of martensite M^\pm (large strain) obtained in tension or compression tests.

Starting from isothermal stress–strain curves obtained in laboratory experiments at very low strain rates, we can associate the strain intervals on which the stress–strain relation has positive slope, both in loading and unloading tests, with the stable phases of the material. Such kind of experiments are illustrated in Shaw [24, Fig. 3] for the pseudoelastic response of a nearly equiatomic polycrystalline NiTi alloy under uniaxial traction tests for temperatures between 15 and 55 °C.

We consider that there exist two critical temperatures θ_m and θ_M with the property that for $\theta \in [\theta_m, \theta_M]$ all three phases are available to the material. This means that, for fixed θ , on the intervals: $\varepsilon \leq \varepsilon_m^-(\theta)$, $\varepsilon \in [\varepsilon_M^-(\theta), \varepsilon_M^+(\theta)]$ and $\varepsilon \geq \varepsilon_m^+(\theta)$, the function $\sigma = \sigma_{eq}(\varepsilon, \theta)$ is a monotonically *increasing* function of strain (Fig. 1). The pairs $(\varepsilon = \varepsilon_M^\pm(\theta), \sigma = \sigma_M^\pm(\theta) = \sigma_{eq}(\varepsilon_M^\pm(\theta), \theta))$ are associated with the change of sign of the slope of the equilibrium stress–strain relation at constant temperature and correspond to the strain–stress states where the instabilities accompanying the $A \rightarrow M^\pm$ phase transformation start to manifest in quasi-static isothermal uniaxial tensile or compressive loading experiments. In fact, they are related to the beginning of the loading stress plateau of the hysteresis loop, which for a NiTi alloy manifests in the form of a first stress drop followed by slight stress oscillations (Shaw [24, Fig. 3]). In a similar way, the pairs $(\varepsilon = \varepsilon_m^\pm(\theta), \sigma = \sigma_m^\pm(\theta) = \sigma_{eq}(\varepsilon_m^\pm(\theta), \theta))$ are associated with the strain–stress states where the instabilities accompanying the reverse $M^\pm \rightarrow A$ phase transformation start to develop along the unloading stress plateau.

For fixed $\theta > \theta_M$, the material only exists in its austenitic form and the stress response function $\sigma = \sigma_{eq}(\varepsilon, \theta)$ is a monotonically *increasing* function of strain. For fixed $\theta < \theta_m$, the material only exists in its martensitic variants M^\pm , and $\sigma = \sigma_{eq}(\varepsilon, \theta)$ is a monotonically *increasing* function of strain for $\varepsilon \leq \varepsilon_m^-(\theta)$ and $\varepsilon \geq \varepsilon_m^+(\theta)$, while on the remaining strain interval $\varepsilon \in (\varepsilon_m^-(\theta), \varepsilon_m^+(\theta))$, it is monotonically *decreasing*.

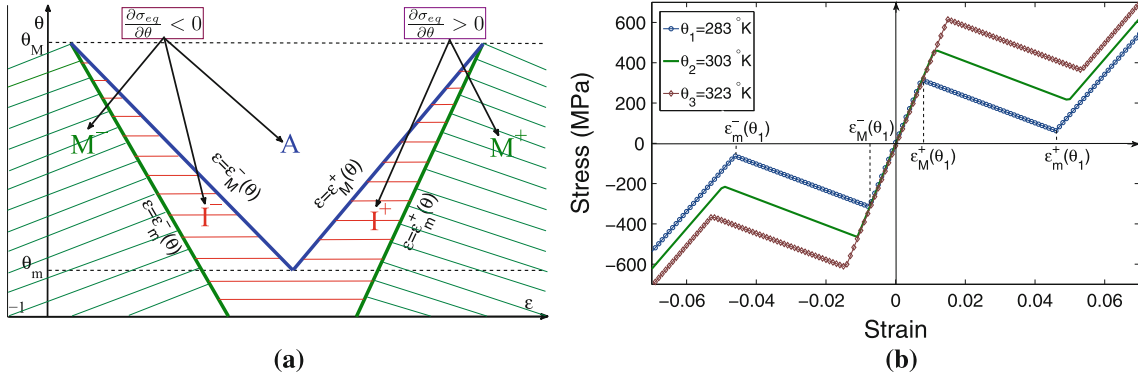


Fig. 1 **a** Schematic description of the phase diagram in the $\varepsilon - \theta$ plane for the piecewise linear thermoelastic model (1)–(3); **b** Evolution of the non-monotone stress–strain relation $\sigma = \sigma_{eq}(\varepsilon, \theta)$ with respect to temperature for the input data in Table 1

Piecewise linear stress–strain relations have been often successfully employed to characterize analytically and numerically different aspects concerning phase transformation in solid bars in the isothermal setting (Abeyaratne and Knowles [18], Truskinovsky [25], Făciu and Molinari [6]) and also in the non-isothermal setting (see Turteltaub [19], Abeyaratne and Knowles [10, 11], Abeyaratne et al. [26], Făciu and Mihăilescu-Suliciu [22], Vainchtein [16]).

We consider in this paper only temperatures θ ranging in an interval included in $[\theta_m, \theta_M]$. The equilibrium stress response function is given by the continuous and piecewise smooth relation

$$\sigma = \sigma_{eq}(\varepsilon, \theta) = \begin{cases} E_3(\varepsilon - \varepsilon_m^-(\theta)) + \sigma_m^-(\theta), & \text{for } \varepsilon \leq \varepsilon_m^-(\theta) \\ -E_2(\varepsilon - \varepsilon_m^-(\theta)) + \sigma_m^-(\theta), & \text{for } \varepsilon_m^-(\theta) < \varepsilon < \varepsilon_M^-(\theta) \\ E_1(\varepsilon - \varepsilon_M^-(\theta)) + \sigma_M^-(\theta), & \text{for } \varepsilon_M^-(\theta) \leq \varepsilon \leq \varepsilon_M^+(\theta) \\ -E_2(\varepsilon - \varepsilon_m^+(\theta)) + \sigma_m^+(\theta), & \text{for } \varepsilon_m^+(\theta) < \varepsilon < \varepsilon_M^+(\theta) \\ E_3(\varepsilon - \varepsilon_m^+(\theta)) + \sigma_m^+(\theta), & \text{for } \varepsilon_M^+(\theta) \leq \varepsilon \end{cases} \quad (1)$$

where $E_1 > 0$ and $E_3 > 0$ represent the constant elastic moduli of the austenite phase A and martensite variants M^\pm , respectively, while $-E_2 < 0$ is the elastic modulus of the unstable (spinodal) regions.

The choice of this simple piecewise linear model is in agreement with the linear thermoelastic behavior observed experimentally for an SMA in uniaxial tensile and compressive tests when the material is in a pure phase: austenite A , or in one of the two martensite variants M^\pm (Shaw [24]). While the monotone increasing parts of the stress–strain relation can be chosen in such a way to fit known quasi-static isothermal experiments, the monotone decreasing part, which induces instability phenomena and influences the kinetics of phase transformation, cannot be determined in a direct way from such tests. For simplicity, we choose here a straight line with constant slope $-E_2$ connecting the local maxima and minima of the equilibrium stress–strain relation.

To get a linear thermoelastic behavior of the material in a single phase, we require that functions $\varepsilon = \varepsilon_M^\pm(\theta)$, $\varepsilon = \varepsilon_m^\pm(\theta)$ as well as $\sigma = \sigma_M^\pm(\theta)$, $\sigma = \sigma_m^\pm(\theta)$ be linear functions of θ . We derive the following expressions (see also [22]):

$$\varepsilon_M^\pm(\theta) = \alpha(\theta - \theta_T) \pm M(\theta - \theta_m), \quad \varepsilon_m^\pm(\theta) = \alpha(\theta - \theta_T) \mp (M - m)(\theta - \theta_M) \pm M(\theta - \theta_m), \quad (2)$$

$$\sigma_M^+(\theta) = -\sigma_M^-(\theta) = E_1 M(\theta - \theta_m), \quad \sigma_m^+(\theta) = -\sigma_m^-(\theta) = E_1 M(\theta - \theta_m) + E_2(M - m)(\theta - \theta_M), \quad (3)$$

satisfying conditions $\varepsilon_M^-(\theta_m) = \varepsilon_M^+(\theta_m)$, $\varepsilon_M^+(\theta_M) = \varepsilon_m^+(\theta_M)$, $\varepsilon_M^-(\theta_M) = \varepsilon_m^-(\theta_M)$ (see Fig. 1a). For simplicity reasons, we have assumed in (3) that the deformation behavior in tension and compression tests is symmetric, although, in general, for SMAs this is not true.

The other material parameters entering (2) have the following meaning. According to (22), $\alpha = \text{const.} > 0$ is the *thermal expansion coefficient* of the material in the austenite phase A , while the temperature $\theta_T \in (\theta_m, \theta_M)$ is a reference temperature with the property that the undeformed material in phase A is stress free, i.e., $\sigma_{eq}(0, \theta_T) = 0$.

Because in traction tests the hysteresis loop moves upwards, while in compression tests, it moves downwards as the temperature grows, it follows that necessarily $\frac{d\sigma_M^+(\theta)}{d\theta}$ and $\frac{d\sigma_m^+(\theta)}{d\theta}$ are positive, while $\frac{d\sigma_M^-(\theta)}{d\theta}$ and $\frac{d\sigma_m^-(\theta)}{d\theta}$ are negative. Moreover, these quantities can be determined experimentally, and it is found that, in general, they

Table 1 Mechanical and thermal parameters for the thermoelastic model

| | | |
|--|---|-----------|
| Elastic modulus of the austenite phase A | E_1 (GPa) | 42 |
| Elastic modulus of the martensite variants M^\pm | E_3 (GPa) | 20 |
| Elastic modulus of the spinodal regions I^\pm | $-E_2$ (GPa) | -6.55 |
| Thermal expansion coefficient in the austenite phase A | α ($^\circ\text{K}^{-1}$) | 10^{-5} |
| Mass density | ρ (kg/m^3) | 8,000 |
| Specific heat in the austenite phase A | C ($\text{J}/\text{Kg}/^\circ\text{C}$) | 500 |

are constant (see Shaw and Kyriakides [27], Shaw [24]). Therefore, the two material constants m and M can be determined from relations $\frac{d\sigma_M^+(\theta)}{d\theta} = E_1 M > 0$ and $\frac{d\sigma_m^+(\theta)}{d\theta} = E_1 M + E_2(M - m) > 0$ once the elastic moduli are known.

In order to study the qualitative as well as quantitative behavior of steady, structured shock and interphase layers in a phase transforming bar, we chose material parameters for the thermoelastic model that ensure a good agreement with the pseudoelastic response of a NiTi strip in traction tests, in the range of temperatures between 15 and 55 $^\circ\text{C}$, considered and illustrated in Shaw [24, Fig. 3]. Table 1 shows the chosen thermal and mechanical constants which, together with the remaining parameters $M = 1.78571 \times 10^{-4} \text{ }^\circ\text{K}^{-1}$, $m = 1.746 \times 10^{-4} \text{ }^\circ\text{K}^{-1}$, $\theta_m = 241.15 \text{ }^\circ\text{K}$, $\theta_M = 10000. \text{ }^\circ\text{K}$, $\theta_T = 293.15 \text{ }^\circ\text{K}$, lead to the isothermal stress-strain curves $\sigma = \sigma_{eq}(\varepsilon, \theta)$ illustrated in Fig. 1b.

The thermoelastic relation (1) is similar to that derived from physical considerations on the behavior of shape memory alloys by Abeyaratne et al. [26]. It has been used in Făciu and Mihăilescu-Suliciu [22] as an equilibrium relation for a Maxwellian rate-type approach to the thermoelasticity and for numerical simulations of quasi-static strain-controlled tests. These simulations of the evolution of the strain and temperature distribution in a specimen have shown a good agreement with the full-field temperature measurements taken by Shaw and Kyriakides [27] in quasi-static laboratory experiments.

Let us note that for the numerical parameters used we get $\frac{d\sigma_M^+(\theta)}{d\theta} = -\frac{d\sigma_M^-(\theta)}{d\theta} = 7.49 \text{ MPa}/^\circ\text{K}$, which is a value appropriate to that obtained experimentally in Shaw [24, Fig. 3] for the rate of increase with respect to the temperature of the stress plateau for $A \rightarrow M^+$ transformation, while $\frac{d\sigma_m^+(\theta)}{d\theta} = -\frac{d\sigma_m^-(\theta)}{d\theta} = 7.52 \text{ MPa}/^\circ\text{K}$.

Moreover, the condition **H3** in Part I [1], which assumes the existence of a monotone curve in the $\varepsilon - \theta$ plane across which $\frac{\partial \sigma_{eq}}{\partial \theta}$ changes its sign, is satisfied. For the numerical entries used, this curve is just $\varepsilon = \varepsilon_M^+(\theta)$ (see Fig. 1a). This property is an essential particular feature of the proposed thermoelastic model, in agreement with the experimental observations, and allows to characterize the thermal dependence of the hysteresis loop in traction or compression tests.

The PDE system describing the motion of a thermoelastic bar in the absence of heat conduction is given by

$$\frac{\partial \varepsilon}{\partial t} - \frac{\partial v}{\partial X} = 0, \quad \rho \frac{\partial v}{\partial t} - \frac{\partial \sigma_{eq}(\varepsilon, \theta)}{\partial X} = 0, \quad \rho C_{eq}(\varepsilon, \theta) \frac{\partial \theta}{\partial t} - \theta \frac{\partial \sigma_{eq}(\varepsilon, \theta)}{\partial \theta} \frac{\partial v}{\partial X} = 0 \quad (4)$$

where $v = v(X, t)$ is the velocity of a particle X at time t . $C_{eq}(\varepsilon, \theta)$ is the *specific heat of the thermoelastic material* and is defined in Appendix A by relation (28).

It is known (see for instance Part I [1]) that the adiabatic thermoelastic system (4) is hyperbolic on those regions of the $\varepsilon - \theta$ plane where $\frac{\partial \sigma_{eq}}{\partial \varepsilon} + \frac{\theta}{\rho C_{eq}} \left(\frac{\partial \sigma_{eq}}{\partial \theta} \right)^2 \geq 0$ and it is elliptic on the complementary part. For the piecewise linear thermoelastic model defined by relations (1)–(3) and for the input data in Table 1, one can verify by using relation (28) in Appendix A that the curves $\varepsilon = \varepsilon_M^\pm(\theta)$ and $\varepsilon = \varepsilon_m^\pm(\theta)$ delimitate the regions of hyperbolicity and ellipticity of the system. We identify the domains of hyperbolicity with the so-called stable phases of the material. These are the *austenite phase* $A = \{(\varepsilon, \theta) | \varepsilon_M^-(\theta) \leq \varepsilon \leq \varepsilon_M^+(\theta)\}$ and the *martensite variants* $M^+ = \{(\varepsilon, \theta) | \varepsilon \geq \varepsilon_M^+(\theta)\}$ and $M^- = \{(\varepsilon, \theta) | \varepsilon \leq \varepsilon_M^-(\theta)\}$ (see Fig. 1). The domains $I^+ = \{(\varepsilon, \theta) | \varepsilon_M^+(\theta) < \varepsilon < \varepsilon_m^+(\theta)\}$ and $I^- = \{(\varepsilon, \theta) | \varepsilon_m^-(\theta) < \varepsilon < \varepsilon_M^-(\theta)\}$, where phase transitions take place, correspond to the elliptic regions of the adiabatic system and are usually called *unstable phases (spinodal regions)* of the material. In these regions, the initial-boundary value problems for the adiabatic system are ill-posed and they are dismissed in a pure thermoelastic approach of phase transitions.

A propagating discontinuity in a thermoelastic material, whose position in the reference configuration is $X = S(t)$, separates the thermomechanical states $v^+, \varepsilon^+, \theta^+$ and $v^-, \varepsilon^-, \theta^-$ and satisfies the following jump conditions and entropy inequality:

$$[[v]] = -\dot{S}[[\varepsilon]], \quad [[\sigma]] = -\rho\dot{S}^2[[\varepsilon]], \quad \dot{S}(\rho[[e_{eq}]] + \langle \sigma \rangle [[\varepsilon]]) = 0, \quad \rho\dot{S}[[\eta_{eq}(\varepsilon, \theta)]] \leq 0, \quad (5.1-4)$$

where $[[f]](t) = f(S(t) + 0, t) - f(S(t) - 0, t)$ and $\langle f \rangle = \frac{1}{2}(f(S(t) + 0, t) + f(S(t) - 0, t))$ denote the jump and the average, respectively, of any field quantity $f(X, t)$ across the discontinuity. This discontinuity corresponds to an *adiabatic thermoelastic shock wave*, or a *phase boundary*, according to whether the particles separated by the discontinuity are in the same phase, or in distinct phases.

Assume that $\dot{S} > 0$ and the thermomechanical state ahead of the shock $(\varepsilon^+, \theta^+)$ is known. Then, the energy jump condition (5.3), known as the Rankine–Hugoniot equation, provides restrictions on the back states $(\varepsilon^-, \theta^-)$ which can be reached in a discontinuous process. The function

$$H(\varepsilon, \theta; \varepsilon^+, \theta^+) = \rho e_{eq}(\varepsilon, \theta) - \rho e^+ - \frac{1}{2}(\sigma_{eq}(\varepsilon, \theta) + \sigma^+)(\varepsilon - \varepsilon^+) \quad (6)$$

is called the *Hugoniot relation based at $(\varepsilon^+, \theta^+)$* where $e^+ = e_{eq}(\varepsilon^+, \theta^+)$ and $\sigma^+ = \sigma_{eq}(\varepsilon^+, \theta^+)$. For our piecewise linear thermoelastic model, it can be explicitly determined as a quadratic function of θ from the expression (30) of the internal energy $e = e_{eq}(\varepsilon, \theta)$ given in Appendix A.

The implicit equation $H(\varepsilon, \theta; \varepsilon^+, \theta^+) = 0$ has in this case a unique global solution with respect to ε called the *temperature–strain Hugoniot locus based at $(\varepsilon^+, \theta^+)$* , i.e.,

$$\theta = \theta_H(\varepsilon; \varepsilon^+, \theta^+) \Leftrightarrow H(\varepsilon, \theta_H(\varepsilon; \varepsilon^+, \theta^+)) = 0 \quad \text{for any } \varepsilon. \quad (7)$$

Its image through the stress response function

$$\sigma = \sigma_H(\varepsilon; \varepsilon^+, \theta^+) \equiv \sigma_{eq}(\varepsilon, \Theta_H(\varepsilon; \varepsilon^+, \theta^+)) \quad (8)$$

is called the *stress–strain Hugoniot locus based at $(\varepsilon^+, \theta^+)$* . Relations (7) and (8) describe all reachable back states $(\varepsilon^-, \theta^-, \sigma^- = \sigma_{eq}(\varepsilon^-, \theta^-))$ in a wave discontinuity which has $(\varepsilon^+, \theta^+, \sigma^+ = \sigma_{eq}(\varepsilon^+, \theta^+))$ as a front state.

3 Augmented theory: Maxwellian rate-type approach

We consider the following Maxwellian rate-type constitutive equation as augmented model of the thermoelastic material (see Part I [1])

$$\frac{\partial \sigma}{\partial t} - E \frac{\partial \varepsilon}{\partial t} = -\frac{E}{\mu}(\sigma - \sigma_{eq}(\varepsilon, \theta)), \quad (9)$$

where $E = \text{const.} > 0$ is called the *dynamic Young modulus*, $\mu = \text{const.} > 0$ is a “viscosity” coefficient and $\sigma = \sigma_{eq}(\varepsilon, \theta)$ is the piecewise linear thermoelastic relation described by (1)–(3). Let us note that $\tau = \frac{\mu}{E}$ is a *relaxation time* of the model.

When we apply this constitutive model to SMAs, it is improper to speak about the “viscosity” of the material. It is better to speak about the relaxation time as a parameter which allows to describe the fact that the transition of a particle from one stable phase to another does not occur instantaneously, but it requires always a finite phase transition time. Due to a certain tradition concerning the terminology related to this constitutive relation and for simplicity reasons in the following, we shall often use the term “viscosity” instead of time of relaxation, or “viscosity effects” instead of “rate-type effects.” In the limit of vanishing relaxation time, this constitutive equation is seen as a rate-type approximation of the thermoelastic model.

The free energy of the constitutive Eq. (9) has been extensively analyzed in Part I [1] (see also [22]). It has been shown that the Maxwellian rate-type model admits a free energy function $\psi = \psi_{Mxw}(\varepsilon, \sigma, \theta)$, uniquely determined by the equilibrium stress–strain–temperature relation $\sigma = \sigma_{eq}(\varepsilon, \theta)$ and by the instantaneous Young’s modulus E (modulo an additive function of temperature) if and only if $\frac{\partial \sigma_{eq}}{\partial \varepsilon} < E$, at the points where the derivative makes sense. It has the form

$$\rho \psi_{Mxw}(\varepsilon, \sigma, \theta) = \frac{\sigma^2}{2E} - \frac{\sigma_{eq}^2(\tilde{\varepsilon}, \theta)}{2E} + \int_{\varepsilon_0}^{\tilde{\varepsilon}} \sigma_{eq}(s, \theta) ds + \rho \phi_1(\theta), \quad (10)$$

Table 2 Mechanical parameters for the augmented theory

| | | |
|-------------------------------|--------------------------------|--------------|
| Dynamic Young's modulus | E (GPa) | 43 or 50 |
| "Viscosity" coefficient | μ (GPa) | 0.0003 ... 3 |
| Heat conductivity coefficient | κ (W/m ² °K) | 0 or 20 |

where $\tilde{\varepsilon} = \tilde{\varepsilon}(\varepsilon, \sigma, \theta)$ is uniquely defined by the algebraic equation

$$\sigma - E\varepsilon = \sigma_{eq}(\tilde{\varepsilon}, \theta) - E\tilde{\varepsilon}. \quad (11)$$

The entropy and the specific heat of the Maxwellian rate-type model are given by $\eta_{Mxw}(\varepsilon, \sigma, \theta) = -\frac{\partial \psi_{Mxw}}{\partial \theta}$ and $C_{Mxw}(\varepsilon, \sigma, \theta) = -\theta \frac{\partial^2 \psi_{Mxw}}{\partial \theta^2}$, respectively, at the points where the derivatives make sense. For the piecewise linear equilibrium relation given by (1)–(3), the expressions of the smooth free energy function, of the discontinuous and piecewise smooth specific heat function, and the continuous and piecewise smooth internal energy function of the Maxwellian rate-type constitutive equation are given in Appendix B.

This rate-type constitutive approach induces an internal dissipation. We also consider here a second dissipative mechanism described by the Fourier law of heat conduction for the axial heat flux $q = -\kappa \frac{\partial \theta}{\partial X}$, where $\kappa = \text{const.} > 0$ is the *heat conductivity coefficient*.

The material data used in this paper to characterize the rate-type effects and the heat transfer effects in the numerical investigation are given in Table 2. We note that the requirements $E_1 < E$ and $E_2 < E$, imposed by the second law of thermodynamics, are satisfied, and the value used for the heat conductivity coefficient κ is an usual one for a SMA.

The PDEs system, in the unknown $v, \varepsilon, \sigma, \theta$ describing the motion of a Maxwellian rate-type phase transforming bar, is composed by the constitutive relation (9), the compatibility equation, the balance of momentum, and the balance of energy

$$\frac{\partial \varepsilon}{\partial t} - \frac{\partial v}{\partial X} = 0, \quad \rho \frac{\partial v}{\partial t} - \frac{\partial \sigma}{\partial X} = 0, \quad (12)$$

$$\rho C_{Mxw} \frac{\partial \theta}{\partial t} = \frac{E}{\mu} \rho \frac{\partial \psi_{Mxw}}{\partial \sigma} (\sigma - \sigma_{eq}(\varepsilon, \theta)) - \frac{E}{\mu} \rho \theta \frac{\partial^2 \psi_{Mxw}}{\partial \theta \partial \sigma} (\sigma - \sigma_{eq}(\varepsilon, \theta)) + \kappa \frac{\partial^2 \theta}{\partial X^2}. \quad (13)$$

One observes here that the variation of the temperature in the diffusion Eq. (13) is determined by the competition between three additive terms in its right-hand side. The first one is related to the *internal dissipation* which always contributes to the increase in the temperature during a thermomechanical process. The second one is related to the *latent heat* released or absorbed by the material and can be positive or negative. The third term is related to the *thermal dissipation* by axial heat conduction.

4 Traveling waves

To investigate the internal structure of a phase boundary, we now seek a solution to the system composed by Eqs. (9), (12), and (13) in the form of traveling wave: $v = \hat{v}(\xi)$, $\varepsilon = \hat{\varepsilon}(\xi)$, $\sigma = \hat{\sigma}(\xi)$, $\theta = \hat{\theta}(\xi)$ where $\xi = X - \hat{S}t$ and $\hat{S} = \text{const.}$ is the speed of the wave. By requiring that the traveling wave connects two equilibrium states behind and in front of the propagating interface, i.e., $(\hat{\varepsilon}, \hat{\sigma}, \hat{\theta}, \hat{v})(\pm\infty) = (\varepsilon^\pm, \sigma^\pm = \sigma_{eq}(\varepsilon^\pm, \theta^\pm), \theta^\pm, v^\pm)$ one gets the following. The limit values of the traveling waves have to satisfy the jump relations (5.1-4) for the associated thermoelastic material. The velocity–strain pairs $(\hat{v}(\xi), \hat{\varepsilon}(\xi))$ belong to a straight line in the $v - \varepsilon$ plane of slope $-\hat{S}$ and the stress–strain pairs $(\hat{\sigma}(\xi), \hat{\varepsilon}(\xi))$ belong to a straight line of slope $\rho \hat{S}^2$ in the $\varepsilon - \sigma$ plane called the *Rayleigh line* and denoted by $\sigma = \sigma_R(\varepsilon)$, i.e.,

$$\hat{v}(\xi) = v^+ - \hat{S}(\hat{\varepsilon}(\xi) - \varepsilon^+), \quad \hat{\sigma}(\xi) = \sigma_R(\hat{\varepsilon}(\xi)) \stackrel{\text{def}}{=} \sigma^+ + \rho \hat{S}^2(\hat{\varepsilon}(\xi) - \varepsilon^+) \quad (14)$$

where $\rho \hat{S}^2 = (\sigma^+ - \sigma^-)/(\varepsilon^+ - \varepsilon^-)$.

The pairs $(\hat{\varepsilon}(\xi), \hat{\theta}(\xi))$ satisfy the dynamical system

$$\begin{aligned} \hat{\varepsilon}' &= -\frac{E}{\mu \hat{S}(E - \rho \hat{S}^2)} R(\hat{\varepsilon}, \hat{\theta}), & \lim_{\xi \rightarrow \pm\infty} \hat{\varepsilon}(\xi) &= \varepsilon^\pm, \\ \hat{\theta}' &= -\frac{\hat{S}}{\kappa} H_{Mxw}(\hat{\varepsilon}, \hat{\theta}), & \lim_{\xi \rightarrow \pm\infty} \hat{\theta}(\xi) &= \theta^\pm, \end{aligned} \quad (15)$$

where, if $\dot{S} > 0$,

$$R(\varepsilon, \theta; \varepsilon^+, \theta^+, \varepsilon^-) \equiv \sigma_R(\varepsilon) - \sigma_{eq}(\varepsilon, \theta) = \sigma^+ + \rho \dot{S}^2 (\varepsilon - \varepsilon^+) - \sigma_{eq}(\varepsilon, \theta), \quad (16)$$

$$H_{Mxw}(\varepsilon, \theta; \varepsilon^+, \theta^+, \varepsilon^-) \equiv \rho e_{Mxw}(\varepsilon, \sigma_R(\varepsilon), \theta) - \rho e^+ - \frac{1}{2}(\varepsilon - \varepsilon^+)(\sigma_R(\varepsilon) + \sigma^+). \quad (17)$$

The states $(\varepsilon^\pm, \theta^\pm)$ are fixed points for the dynamical system and they are the intersection points between the curves $R(\varepsilon, \theta) = 0$ and the Hugoniot locus $H(\varepsilon, \theta) = 0$ in the $\varepsilon - \theta$ plane. The pairs $(\varepsilon^\pm, \sigma^\pm)$ represent the intersection points of the Rayleigh line $\sigma = \sigma_R(\varepsilon)$ with the stress–strain Hugoniot curve $\sigma = \sigma_H(\varepsilon; \varepsilon^+, \theta^+)$ in the $\varepsilon - \sigma$ plane.

The topological properties of the curve $H_{Mxw}(\varepsilon, \theta) = 0$ and $R(\varepsilon, \theta) = 0$ characterize the main features of the profile layers defined by the Maxwellian rate-type constitutive equation (9) and/or by the Fourier heat conduction law, respectively. They have been qualitatively investigated in Part I [1] where thermodynamical aspects have been put into evidence. Thus, according to (15), the set $\{(\varepsilon, \theta) | H_{Mxw}(\varepsilon, \theta; \varepsilon^+, \theta^+, \varepsilon^-) = 0\}$ describes the trajectory in the $\varepsilon - \theta$ plane of a traveling wave solution structured only by the time of relaxation $\frac{\mu}{E}$ (or, equivalently by the “viscosity” μ) in the absence of heat conduction, i.e., when $\kappa = 0$. Since $\frac{\partial H_{Mxw}}{\partial \theta} = C_{Mxw}(\varepsilon, \sigma_R(\varepsilon), \theta) > 0$, this set can be uniquely represented as a curve-like function connecting the front and the back states $(\varepsilon^\pm, \theta^\pm)$, i.e.,

$$\theta = \Theta_{Mxw}(\varepsilon; \varepsilon^+, \theta^+, \varepsilon^-) \Leftrightarrow H_{Mxw}(\varepsilon, \Theta_{Mxw}(\varepsilon; \varepsilon^+, \theta^+, \varepsilon^-)) = 0 \quad \text{for } \varepsilon \text{ between } \varepsilon^+ \text{ and } \varepsilon^-. \quad (18)$$

Moreover, the image of this curve through the equilibrium relation $\sigma = \sigma_{eq}(\varepsilon, \theta)$ is given by the function

$$\sigma = \sigma_{Mxw}(\varepsilon; \varepsilon^+, \theta^+, \varepsilon^-) \equiv \sigma_{eq}(\varepsilon, \Theta_{Mxw}(\varepsilon; \varepsilon^+, \theta^+, \varepsilon^-)), \quad (19)$$

which connects the front and back states $(\varepsilon^\pm, \sigma^\pm)$ in the $\varepsilon - \sigma$ plane.

If we denote by $\Pi(\hat{\varepsilon}(\xi)) = (\hat{\varepsilon}(\xi), \sigma_R(\hat{\varepsilon}(\xi)), \Theta_{Mxw}(\hat{\varepsilon}(\xi)))$ the trajectory of a “viscous,” heat non-conducting traveling wave solution in the $\varepsilon - \sigma - \theta$ space, one derives the following relation (see Part I [1, Sect. 5.1.2]):

$$\frac{d\Theta_{Mxw}(\varepsilon)}{d\varepsilon} = \frac{E - \rho \dot{S}^2}{E \rho C_{Mxw}(\Pi(\varepsilon))} \left(\sigma_R(\varepsilon) - \sigma_{eq}(\tilde{\varepsilon}, \Theta_{Mxw}(\varepsilon)) + \frac{E \Theta_{Mxw}(\varepsilon)}{E - \frac{\partial \sigma_{eq}(\tilde{\varepsilon}, \Theta_{Mxw}(\varepsilon))}{\partial \varepsilon}} \frac{\partial \sigma_{eq}(\tilde{\varepsilon}, \Theta_{Mxw}(\varepsilon))}{\partial \theta} \right), \quad (20)$$

where $\tilde{\varepsilon} = \tilde{\varepsilon}(\varepsilon)$ is the unique solution of Eq. (11) for $\sigma = \sigma_R(\varepsilon)$ and $\theta = \Theta_{Mxw}(\varepsilon)$. The difference $\sigma_R(\varepsilon) - \sigma_{eq}(\tilde{\varepsilon}, \Theta_{Mxw}(\varepsilon))$ is related with the internal dissipation, while the last term in the right parenthesis is related to the latent heat released or absorbed inside the layer and depends essentially on the sign of $\frac{\partial \sigma_{eq}}{\partial \theta}$. Therefore, the temperature variation inside a “viscous,” heat non-conducting profile layer has two additive sources: the internal dissipation, which always contributes to the increase in the temperature inside the layer, and the latent heat which can act in both senses, i.e., to increase or decrease the temperature. Let also note that, in order to establish from the above relations whether the temperature inside the layer increases or decreases between ε^- and ε^+ , we have to take into account whether the forward propagating traveling wave ($\dot{S} > 0$) is compressive ($\varepsilon^- < \varepsilon^+$) or expansive ($\varepsilon^- > \varepsilon^+$).

For our piecewise linear equilibrium relations (1)–(3), the function $H_{Mxw}(\varepsilon, \theta; \varepsilon^+, \theta^+, \varepsilon^-)$ given by relation (17) is quadratic in θ and ε and has been calculated using the internal energy (34) given in Appendix B. From here, the function $\theta = \Theta_{Mxw}(\varepsilon; \varepsilon^+, \theta^+, \varepsilon^-)$ has been explicitly obtained as a continuous and piecewise C^1 function.

In the absence of “viscosity,” i.e., when $\mu = 0$, a traveling wave solution structured only by heat conduction has to satisfy the reduced system

$$R(\hat{\varepsilon}, \hat{\theta}) = 0, \quad \text{and} \quad \hat{\theta}' = -\frac{\dot{S}}{\kappa} H_{Mxw}(\hat{\varepsilon}, \hat{\theta}), \quad \lim_{\xi \rightarrow \pm\infty} \hat{\theta}(\xi) = \theta^\pm. \quad (21.1-3)$$

Thus, the set $\{(\varepsilon, \theta) | R(\varepsilon, \theta; \varepsilon^+, \theta^+, \varepsilon^-) = 0\}$, called the Rayleigh set in the $\varepsilon - \theta$ plane, corresponds to the trajectory in the $\varepsilon - \theta$ plane of a “non-viscous,” heat conducting traveling wave solution. It has been shown in Part I [1] and it is illustrated in the numerical examples below that there exists a major difference in the effect of “viscosity” and heat conduction on the structure of the profile layers in the sense that a “non-viscous,” heat

conducting profile layer, solution of problem (21.1-3), in general, sweeps only some portions of the Rayleigh set leading to the so-called isothermal jumps in strain and stress inside the profile layers.

Since $\frac{\partial R(\varepsilon, \theta)}{\partial \varepsilon} = -\frac{\partial \sigma_{eq}}{\partial \theta}$, it follows that the Rayleigh set, i.e., the solution of the implicit equation $R(\varepsilon, \theta) = 0$, is uniquely representable as a function $\theta = \Theta_R(\varepsilon; \varepsilon^+, \theta^+, \varepsilon^-)$ connecting the front and back states $(\varepsilon^\pm, \theta^\pm)$ if $\frac{\partial \sigma_{eq}}{\partial \theta}$ has a constant sign in a domain containing $(\varepsilon^\pm, \theta^\pm)$. Moreover, its image through the equilibrium stress response function $\sigma = \sigma_{eq}(\varepsilon, \theta)$ is the Rayleigh line, i.e., $\sigma_R(\varepsilon) = \sigma_{eq}(\varepsilon, \Theta_R(\varepsilon; \varepsilon^+, \theta^+, \varepsilon^-))$. For the piecewise linear stress response function (1)–(3), the function $\theta = \Theta_R(\varepsilon; \varepsilon^+, \theta^+, \varepsilon^-)$ is a continuous and piecewise linear function. When $\frac{\partial \sigma_{eq}}{\partial \theta}$ changes its sign only once in a domain containing $(\varepsilon^\pm, \theta^\pm)$, then the Rayleigh set is a disconnected set representable by two functions of ε , one $\theta = \Theta_R^+(\varepsilon)$ passing through $(\varepsilon^+, \theta^+)$ and the other $\theta = \Theta_R^-(\varepsilon)$ passing through $(\varepsilon^-, \theta^-)$.

Admissibility condition. In Part I [1, Sect. 5.1], it has been shown that a *chord criterion with respect to the curve* $\sigma = \sigma_{Mxw}(\varepsilon; \varepsilon^+, \theta^+, \varepsilon^-)$ defined by (19) is, in general, a necessary and sufficient condition for the existence of a unique solution for the nonlinear autonomous system (15). This is also an admissibility condition for the selection of physical relevant jump discontinuities for the associated adiabatic thermoelastic system (4). Moreover, it has been shown that this condition is equivalent with a *chord condition with respect to the stress–strain Hugoniot locus* $\sigma = \sigma_H(\varepsilon; \varepsilon^+, \theta^+)$ defined by (8). Thus, the problem of the existence and uniqueness of a solution for the problem (15) has been reduced to a condition which only depends on the energetic properties of the associated thermoelastic model.

This selection criterion claims: if $\dot{S} > 0$ and the front state is $(\varepsilon^+, \theta^+)$ and the Hugoniot back state is $(\varepsilon^-, \theta^-)$ then a *compressive wave discontinuity*, i.e., $\varepsilon^+ > \varepsilon^-$, is admissible if and only if the Rayleigh line $\sigma_R(\varepsilon)$ which joins $(\varepsilon^+, \sigma^+ = \sigma_{eq}(\varepsilon^+, \theta^+))$ to $(\varepsilon^-, \sigma^- = \sigma_{eq}(\varepsilon^-, \theta^-))$ lies *below* the graph of the function $\sigma = \sigma_H(\varepsilon; \varepsilon^+, \theta^+)$ for $\varepsilon \in (\varepsilon^-, \varepsilon^+)$, while an *expansive wave discontinuity*, i.e., $\varepsilon^+ < \varepsilon^-$, is admissible if and only if the Rayleigh line $\sigma_R(\varepsilon)$ lies *above* the graph of the Hugoniot locus for $\varepsilon \in (\varepsilon^+, \varepsilon^-)$. If $\dot{S} < 0$, the front state is $(\varepsilon^-, \theta^-)$ and the Hugoniot back state is $(\varepsilon^+, \theta^+)$ then the above statement remains valid if one inverts the superscripts + with –.

5 Numerical results and discussions

The heating or the cooling of a transformed zone in a high strain-rate test is a main characteristic of a phase transforming material like SMA. Therefore, in an impact experiment, a phase boundary will start to propagate, and a large variation of the temperature should appear across it. This could be detected by infrared measurements providing a valuable hint concerning the propagation of a phase boundary. That is why, in the following, we investigate, for a model built in agreement with experimental data, how large is the variation of the temperature across such a phase boundary and how the internal dissipation and the latent heat influences the profile of the temperature inside the layer.

5.1 Compressive $A \rightarrow M^-$ interphase layers ($\frac{\partial \sigma_{eq}(\varepsilon^\pm, \theta^\pm)}{\partial \theta} < 0$)

Let us investigate the internal structure of the traveling wave solutions for a compressive $A \rightarrow M^-$ impact-induced interphase layer when at the front and back state and inside the profile layer we have $\frac{\partial \sigma_{eq}}{\partial \theta} < 0$. This condition corresponds to the classical case investigated in the framework of thermoelastic fluids (see for instance Gilbarg [28], Pego [29]) where the variation of the pressure p with respect to the temperature is positive, i.e., $\frac{\partial p}{\partial \theta} > 0$.

We consider the front state $(\varepsilon^+, \theta^+)$ at the boundary between phase A and the unstable region I^- , i.e., $\varepsilon^+ = \varepsilon_M^-(\theta^+)$ (Fig. 3). That means, the strain–stress front state is located at the point $(\varepsilon^+, \sigma^+ = \sigma_M^-(\theta^+))$ where the slope with respect to the strain of the isotherm $\sigma = \sigma_{eq}(\varepsilon, \theta^+)$ changes its sign (Fig. 2). Any back state $(\varepsilon^-, \theta^-)$ has to lie on the temperature–strain Hugoniot locus based at $(\varepsilon^+, \theta^+)$, i.e., it satisfies relation $\theta = \theta_H(\varepsilon; \varepsilon^+, \theta^+)$ (Fig. 3), while the back state $(\varepsilon^-, \sigma^-)$ lies on the stress–strain Hugoniot locus $\sigma = \sigma_H(\varepsilon; \varepsilon^+, \theta^+)$ based at $(\varepsilon^+, \sigma^+)$ (Fig. 2). We consider five different back states in the phase M^- $(\varepsilon_i^-, \theta_i^-)$, $i = 1, \dots, 5$, and in all cases, the chord criterion with respect to the stress–strain Hugoniot locus $\sigma = \sigma_H(\varepsilon; \varepsilon^+, \theta^+)$ based at $(\varepsilon^+, \sigma^+)$ is satisfied, i.e., the Rayleigh line lies always below the Hugoniot locus for $\varepsilon \in (\varepsilon_i^-, \varepsilon^+)$. This

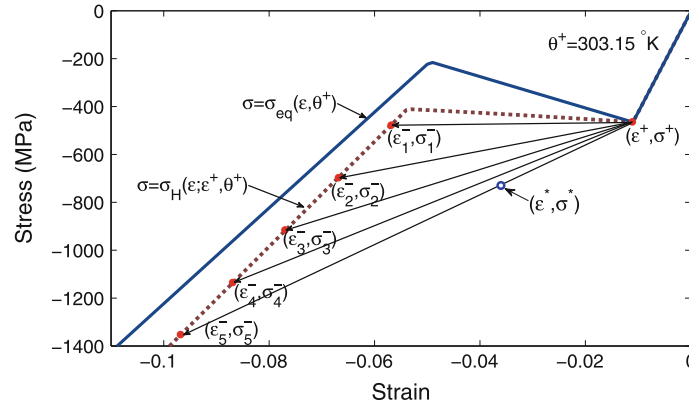


Fig. 2 The stress–strain Hugoniot locus based at $(\varepsilon^+, \sigma^+)$, $\sigma = \sigma_H(\varepsilon; \varepsilon^+, \theta^+)$ and the Rayleigh lines corresponding to five admissible compressive jump discontinuities $(\varepsilon_i^-, \theta_i^-)$, $i = 1, \dots, 5$ from phase A to martensitic variant M^-

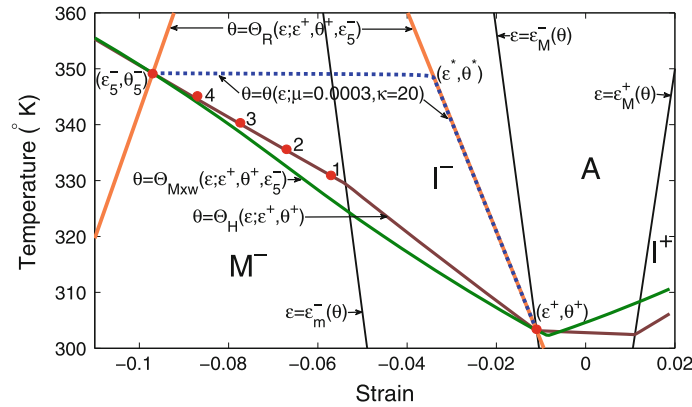


Fig. 3 $A \rightarrow M^-$ interphase layers in the phase diagram; the temperature–strain Hugoniot locus based at $(\varepsilon^+, \theta^+)$, $\theta = \theta_H(\varepsilon; \varepsilon^+, \theta^+)$; the explicit solutions $\theta = \Theta_R(\varepsilon; \varepsilon^+, \theta^+, \varepsilon_5^-)$ and $\theta = \Theta_{Mxw}(\varepsilon; \varepsilon^+, \theta^+, \varepsilon_5^-)$ of the implicit equations $R = 0$ and $H_{Mxw} = 0$ given by Eqs. (16) and (17), respectively

condition ensures the existence and uniqueness of a solution of the system (15), for any $\mu > 0$ and $\kappa > 0$ (see Part I [1, Sect. 5.2]).

Let us denote by $(\hat{\varepsilon}(\xi; \mu, \kappa), \hat{\theta}(\xi; \mu, \kappa))$ such a traveling wave solution and by $\theta = \Theta(\varepsilon; \mu, \kappa)$ its trajectory in the temperature–strain plane. We consider in Fig. 3 for the back state $\varepsilon^- = \varepsilon_5^-$ two extreme situations. First, the trajectory of a “viscous” ($\mu > 0$), heat non-conducting ($\kappa = 0$) traveling wave solution $\theta = \Theta(\varepsilon; \mu, 0)$. This is just the curve $\theta = \Theta_{Mxw}(\varepsilon; \varepsilon^+, \theta^+, \varepsilon_5^-)$ defined by relation (18). Second, we consider the case when the “viscosity” effect is practically negligible with respect to the heat conductivity effect and we plot the trajectory $\theta = \Theta(\varepsilon; \mu = 0.0003 \text{ GPa s}, \kappa = 20 \text{ W/m}^2\text{K})$.

The function $\theta = \Theta_{Mxw}(\varepsilon; \varepsilon^+, \theta^+, \varepsilon_i^-)$ has to be monotone decreasing for $\varepsilon \in (\varepsilon_i^-, \varepsilon^+)$, $i = 1, \dots, 5$. This follows from relation (20) as a consequence of the fact that the chord condition $\sigma_R(\varepsilon) < \sigma_{Mxw}(\varepsilon)$ implies $\sigma_R(\varepsilon) < \sigma_{eq}(\hat{\varepsilon}(\varepsilon), \Theta_{Mxw}(\varepsilon))$, for $\varepsilon \in (\varepsilon_i^-, \varepsilon^+)$, $i = 1, \dots, 5$ (see Part I [1, Sect. 5.2.1 Case C1]) and on the other side, because $\frac{\partial \sigma_{eq}}{\partial \theta} < 0$ in phase M^- and in the spinodal region I^- . According to the remarks following relation (20) this means that both the internal dissipation and the latent heat lead to the increase in the temperature inside a “viscous,” heat non-conducting interphase layer. Thus, after the passage of a wave, the back state temperature is larger than the front state temperature, i.e., $\theta_i^- > \theta^+$, $i = 1, \dots, 5$. The structure of the “viscous,” heat non-conducting interphase layers corresponding to the five compressive jumps is illustrated in Fig. 4. The way in which the back state temperature increases as the absolute value of the back strain increases and the corresponding values of the propagation speed of the phase boundary is illustrated in Table 3.

We say that these compressive waves are of *heating type*. The significant rise of the temperature after the passage of the moving phase boundary is due to the latent heat released by the material in this dynamic process and expresses the *exothermic* character of $A \rightarrow M^-$ phase transformation. In fact, it is a consequence of the

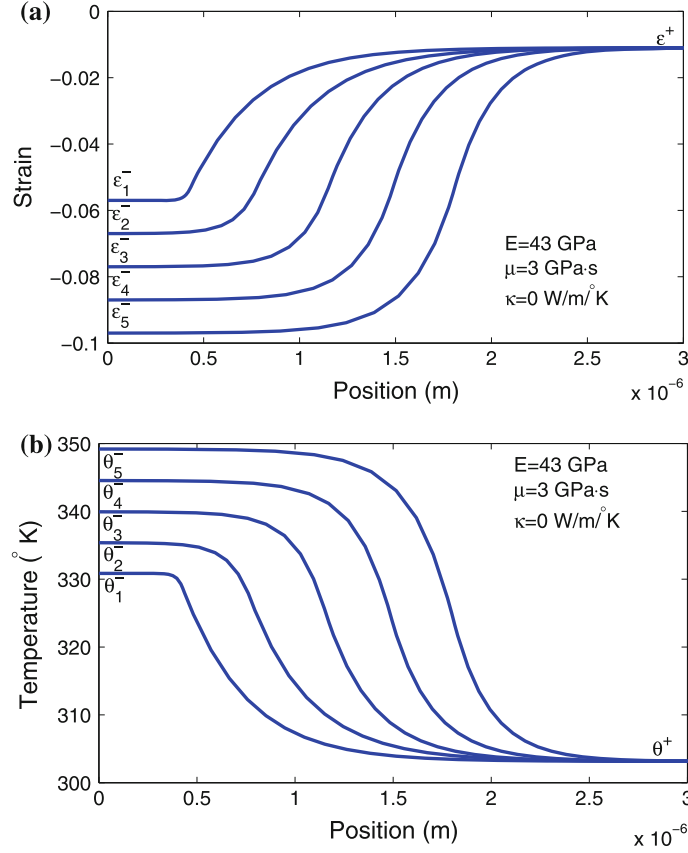


Fig. 4 Structure of “viscous,” heat-non-conducting interphase layers corresponding to the compressive jumps in Figs. 2 and 3

Table 3 Back states and phase boundary speed \dot{S} when the front state is $(\varepsilon^+ = -0.011, \theta^+ = 303.15^\circ\text{K}, \sigma^+ = -464 \text{ MPa})$

| Back state | 1 | 2 | 3 | 4 | 5 |
|--|--------|--------|--------|--------|--------|
| ε^- | -0.057 | -0.067 | -0.077 | -0.087 | -0.097 |
| θ^- ($^\circ\text{K}$) | 330.8 | 335.3 | 339.9 | 344.5 | 349.1 |
| $\sigma^- = \sigma_{eq}(\varepsilon^-, \theta^-)$ (MPa) | -480 | -699 | -918 | -1,138 | -1,358 |
| $\dot{S} = \sqrt{\frac{\sigma^+ - \sigma^-}{\rho(\varepsilon^+ - \varepsilon^-)}}$ (m/s) | 206 | 724 | 927 | 1,052 | 1,139 |

large variation of the equilibrium stress response function with respect to the temperature. Indeed, $\frac{\partial \sigma_{eq}}{\partial \theta} = -8.6 \text{ MPa}/^\circ\text{K}$ in the unstable region I^- and $\frac{\partial \sigma_{eq}}{\partial \theta} = -4.2 \text{ MPa}/^\circ\text{K}$ in the phase M^- .

Let us consider the opposite case when the heat conductivity effect is much more important than the “viscosity” effect. First, we observe in the phase diagram in Fig. 3 that the Rayleigh set, $\theta = \Theta_R(\varepsilon; \varepsilon^+, \theta^+, \varepsilon_5^-)$, solution of the implicit equation (21.1) is non-monotone. Second, we recall that in this case the trajectory $\theta = \Theta(\varepsilon; \mu, \kappa)$ of a traveling wave solution of the problem (15) has to be monotonously decreasing for any $\mu > 0$ and $\kappa > 0$ for $\varepsilon \in (\varepsilon^-, \varepsilon^+)$ in Fig. 3 (see Part I [1, Sect. 5.2.1]). Moreover, for a fixed heat conductivity $\kappa = \bar{\kappa}$ and $\mu \rightarrow 0$, the trajectories $\theta = \Theta(\varepsilon; \mu, \kappa)$ are increasingly close to the monotone descending parts of the curve $\theta = \Theta_R(\varepsilon)$ and approach the solution of the reduced system (21.1-3).

For $\kappa = 20 \text{ W/m}^\circ\text{K}$ and $\mu = 0.0003 \text{ GPa}\cdot\text{s}$ the trajectory of the traveling wave solution is represented by a dotted line in the phase diagram in Fig. 3. It is composed by a nearly horizontal line which starts at the back state $(\varepsilon_5^-, \theta_5^-)$, passes very close to a state $(\varepsilon^*, \theta^*)$, where $\theta_5^- = \Theta_R(\varepsilon^*)$ and is followed by a curve extremely close to the curve $\theta = \Theta_R(\varepsilon)$ and ends at the front state $(\varepsilon^+, \theta^+)$.

The corresponding structure of the strain, temperature, and stress interphase layer is represented in Fig. 5. This numerical example illustrates that when the only structuring mechanism is the heat conduction, the internal structure of a “non-viscous,” heat conducting interphase layer can contain *isothermal jumps in strain*

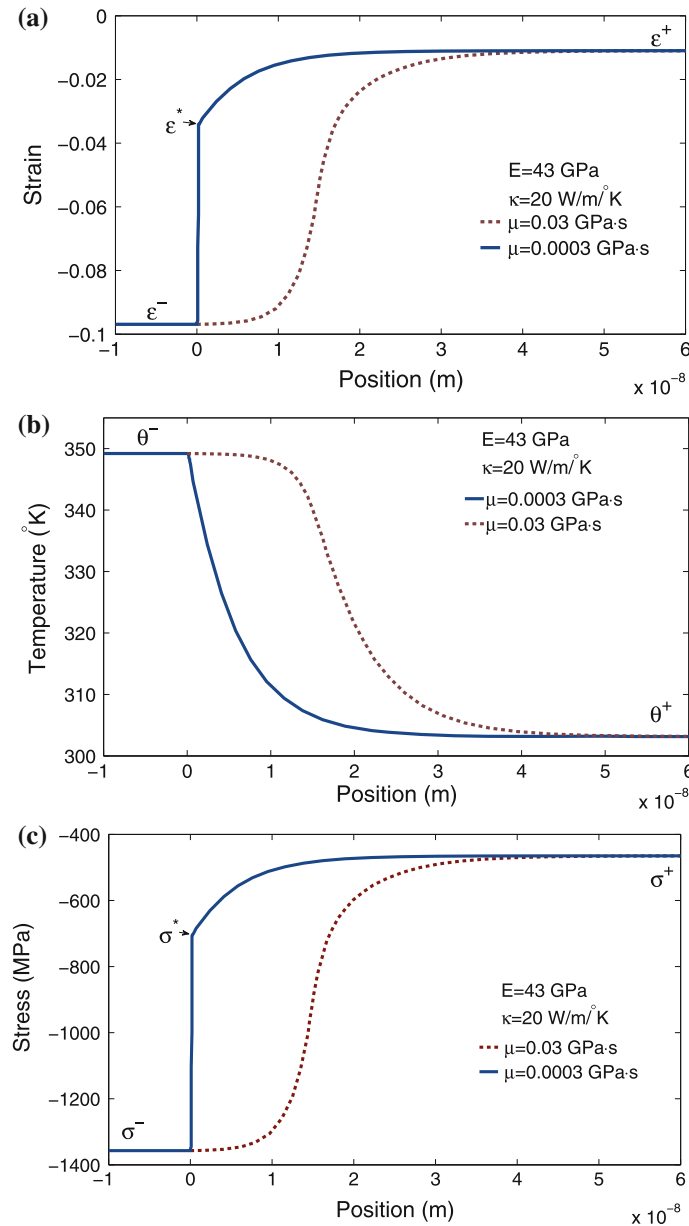


Fig. 5 Structure of interphase layers when the conductivity effect dominates the “viscosity” effect for the back strain $\varepsilon^- = \varepsilon_5^-$ in Figs. 2 and 3

and stress inside the layer. Indeed, one observes in Fig. 5a,c that the interphase layer approximates a jump in strain from ε_5^- to ε^* and a jump in stress from σ_5^- to $\sigma^* = \sigma_R(\varepsilon^*) = \sigma^+ + \rho \dot{S}^2(\varepsilon^* - \varepsilon^+)$. Therefore, in this case, the trajectory of an interphase layer in the stress–strain plane sweeps the portion of the Rayleigh line ranging from ε^+ to ε^* and is followed by a jump from $(\varepsilon^*, \sigma^*)$ to $(\varepsilon_5^-, \theta_5^-)$ (Fig. 2).

Let us note in Fig. 6 that the entropy of the Hugoniot back state $(\varepsilon^-, \theta^-)$ is larger than the entropy of the front state $(\varepsilon^+, \theta^+)$. Therefore, this jump discontinuity is compatible with the second law of thermodynamics. On the other hand, if one investigates the influence of the “viscosity” and of the heat conductivity on the behavior of the entropy inside an interphase layer, one observes an important difference on their structuring role. Indeed, when the “viscosity” effect dominates the heat conductivity effect then the variation of entropy inside the profile layer is monotone (Fig. 6a). In the opposite case, when the heat conductivity effect dominates the “viscosity” effect, then the entropy variation is non-monotone, and even more its values can become inside the profile layer larger than the entropy of the Hugoniot back state (Fig. 6b). This phenomenon is known as

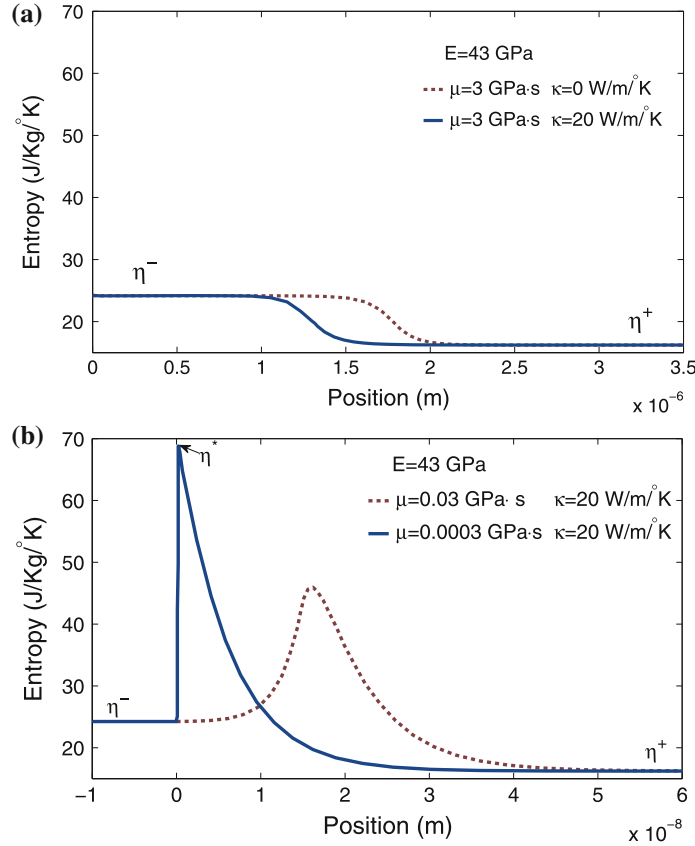


Fig. 6 Entropy variation inside $A \rightarrow M^-$ interphase layers. **a** Monotone variation—the “viscosity” effect dominates the conductivity effect. **b** Non-monotone variation and “overshoot” phenomenon—the conductivity effect dominates the “viscosity” effect

the “entropy overshoot.” It has been reported for instance by Landau and Lifschitz [30, Chap. IX, §87] in gas dynamics and by Dunn and Fosdick [23] in thermoelastic materials. Let also note in Fig. 6b that when the heat conduction is the only structuring parameter of the interphase layer, the entropy can have a jump inside the layer from η^- to $\eta^* = \eta_{\text{Mxw}}(\varepsilon^*, \sigma^*, \theta^*)$.

5.2 Expansive $M^- \rightarrow A$ interphase layers ($\frac{\partial \sigma_{eq}(\varepsilon^\pm, \theta^\pm)}{\partial \theta} < 0$)

We analyze now thermomechanical features of the interphase layers in the expansive case, i.e., $\varepsilon^+ < \varepsilon^-$, corresponding to impact-induced $M^- \rightarrow A$ phase transformations. Inside the profile layer, we have again $\frac{\partial \sigma_{eq}}{\partial \theta} < 0$. We consider the front state $(\varepsilon^+, \theta^+)$ located at the boundary between phase M^- and the unstable region I^- , i.e., $\varepsilon^+ = \varepsilon_m^-(\theta^+)$ (Fig. 8). That means, the strain–stress front state is located at the point $(\varepsilon^+, \sigma^+ = \sigma_m^-(\theta^+))$ where the slope with respect to the strain of the isotherm $\sigma = \sigma_{eq}(\varepsilon, \theta^+)$ changes its sign (Fig. 7). This also corresponds to a local maximum of the Hugoniot stress–strain relation $\sigma = \sigma_H(\varepsilon; \varepsilon^+, \theta^+)$. Any back state $(\varepsilon^-, \theta^-)$ lies on the temperature–strain Hugoniot locus based at $(\varepsilon^+, \theta^+)$, $\theta = \theta_H(\varepsilon; \varepsilon^+, \theta^+)$ (Fig. 8), while the back state $(\varepsilon^-, \sigma^-)$ lies on the stress–strain Hugoniot locus $\sigma = \sigma_H(\varepsilon; \varepsilon^+, \theta^+)$ based at $(\varepsilon^+, \sigma^+)$ (Fig. 7). We consider four different back states in phase A $(\varepsilon_i^-, \theta_i^-)$, $i = 1, \dots, 4$ and in all cases, the chord criterion with respect to the stress–strain Hugoniot locus $\sigma = \sigma_H(\varepsilon; \varepsilon^+, \theta^+)$ is satisfied, i.e., the Rayleigh line lies always above the Hugoniot locus for $\varepsilon \in (\varepsilon^+, \varepsilon_i^-)$.

We consider here only “viscous,” heat non-conducting interphase layers. Their trajectories in the phase diagram plane, corresponding to the four considered back states, are given by the curves $\theta = \Theta_{\text{Mxw}}(\varepsilon; \varepsilon^+, \theta^+, \varepsilon_i^-)$, $i = 1, \dots, 4$ illustrated in Fig. 8. Their images $\sigma = \sigma_{\text{Mxw}}(\varepsilon; \varepsilon^+, \theta^+, \varepsilon_i^-)$, $i = 1, \dots, 4$ in the stress–strain plane defined by relation (19) are illustrated in Fig. 7. One sees that the chord criterion with

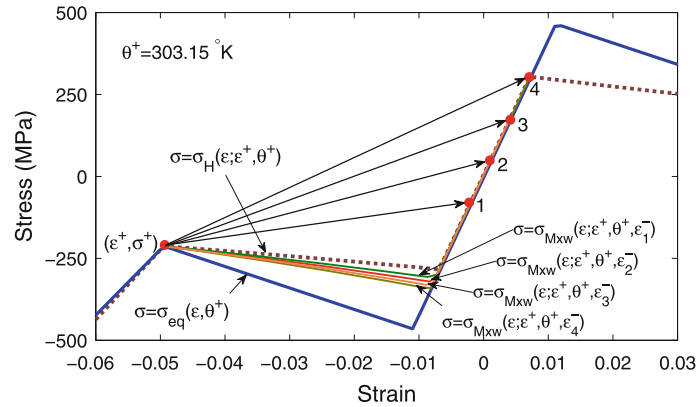


Fig. 7 The stress–strain Hugoniot locus based at $(\varepsilon^+, \sigma^+)$, $\sigma = \sigma_H(\varepsilon; \varepsilon^+, \theta^+)$ and the Rayleigh lines corresponding to four admissible expansive jump discontinuities $(\varepsilon_i^-, \theta_i^-)$, $i = 1, \dots, 4$ from martensitic variant M^- to phase A

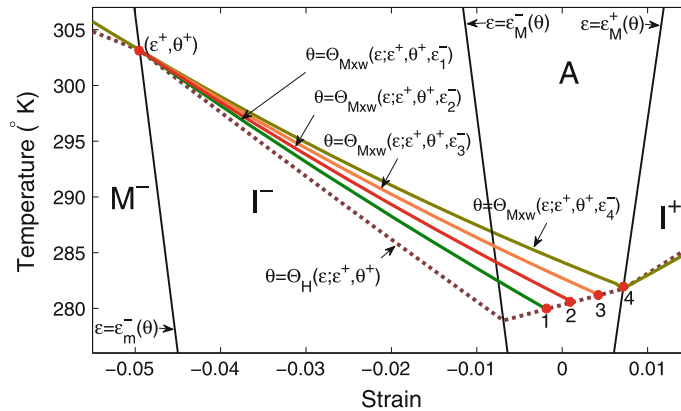


Fig. 8 $M^- \rightarrow A$ interphase layers in the phase diagram; the temperature–strain Hugoniot locus based at $(\varepsilon^+, \theta^+)$, $\theta = \theta_H(\varepsilon; \varepsilon^+, \theta^+)$; the trajectories of the “viscous” ($\mu > 0$), heat non-conducting ($\kappa = 0$) traveling wave solutions $\theta = \theta_{Mxw}(\varepsilon; \varepsilon^+, \theta^+, \varepsilon_i^-)$, $i = 1, \dots, 4$

respect to these curves is also satisfied, that is, the Rayleigh lines connecting the front state $(\varepsilon^+, \sigma^+)$ and the back state $(\varepsilon_i^-, \sigma_i^-)$ lie always above the curve $\sigma = \sigma_{Mxw}(\varepsilon; \varepsilon^+, \theta^+, \varepsilon_i^-)$, for $\varepsilon \in (\varepsilon^+, \varepsilon_i^-)$, $i = 1, \dots, 4$.

In this case, the internal dissipation and the latent heat act in opposite sense. Thus, while the internal dissipation is a source of heating, the latent heat is a source of cooling inside the interphase layer. Indeed, the first term in relation (20) is positive because the chord condition $\sigma_R(\varepsilon) > \sigma_{Mxw}(\varepsilon; \varepsilon^+, \theta^+, \varepsilon_i^-)$, for $\varepsilon \in (\varepsilon_i^-, \varepsilon^+)$, $i = 1, \dots, 4$ is fulfilled, but the second term is negative because $\frac{\partial \sigma_{eq}}{\partial \theta} < 0$ along the traveling wave solution. Since the calculated functions $\theta = \theta_{Mxw}(\varepsilon; \varepsilon^+, \theta^+, \varepsilon_i^-)$ in Fig. 8 are strictly decreasing for $\varepsilon \in (\varepsilon^+, \varepsilon_i^-)$, $i = 1, \dots, 4$, it results that the cooling due to the latent heat absorbed by the material inside the interphase layer dominates the heating due to the internal dissipation. Therefore, after the passage of the wave, the back state temperature decreases considerably, i.e., $\theta_i^- < \theta^+$, $i = 1, \dots, 4$. We say that these expansive waves are of *cooling type*.

The structure of the strain and temperature interphase layers when the only structuring mechanism is the “viscosity” corresponding to the four expansive jumps is illustrated in Fig. 9. The way in which the back state temperature changes as the back strain increases and the corresponding values of the propagation speed of the phase boundary is illustrated in Table 4.

The decrease in the back state temperature after the passage of the wave is obviously due to the latent heat absorbed by the material inside the interphase layer. Even in the case of a phase boundary propagating with the small speed of 28 m/s (see for instance case 0 in Table 4), the temperature drops by more than 24 °K. This behavior is natural and in agreement with the fact that the $M^- \rightarrow A$ phase transformation is *endothermic*.

On the other side, one notes that the back state temperature θ_i^- increases as the back state strain ε_i^- increases. This is because the internal dissipation is proportional with the area between the Rayleigh line and the curve

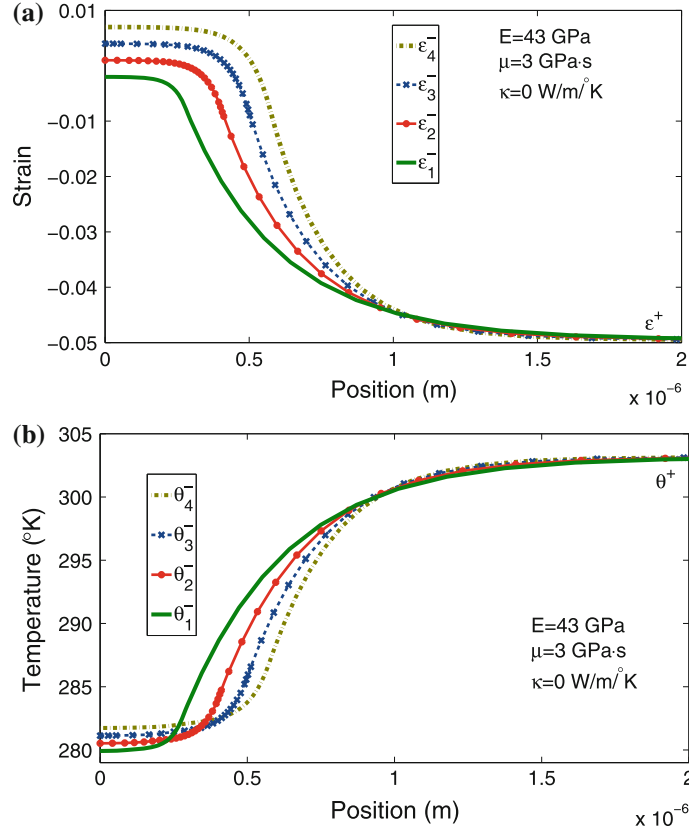


Fig. 9 Structure of “viscous,” heat non-conducting interphase layers corresponding to the four expansive jumps in Figs. 7 and 8

Table 4 Back states and phase boundary speed \dot{S} when the front state is ($\varepsilon^+ = -0.05$, $\theta^+ = 303.15^\circ\text{K}$, $\sigma^+ = -223.2$ MPa)

| Back state | 0 | 1 | 2 | 3 | 4 |
|--|---------|--------|-------|-------|-------|
| ε^- | -0.0054 | -0.002 | 0.001 | 0.004 | 0.007 |
| θ^- ($^\circ\text{K}$) | 278.9 | 279.7 | 280.3 | 280.9 | 281.5 |
| $\sigma^- = \sigma_{eq}(\varepsilon^-, \theta^-)$ (MPa) | -222.9 | -78.4 | 47.3 | 173.0 | 298.8 |
| $\dot{S} = \sqrt{\frac{\sigma^+ - \sigma^-}{\rho(\varepsilon^+ - \varepsilon^-)}}$ (m/s) | 28 | 614 | 814 | 957 | 1,070 |

$\sigma = \sigma_{\text{Mxw}}(\varepsilon; \varepsilon^+, \theta^+, \varepsilon_i^-)$ for $\varepsilon \in (\varepsilon^+, \varepsilon_i^-)$, $i = 1, \dots, 4$. As the strain increases, the corresponding area also increases, and consequently the contribution of the internal dissipation to the heating inside the interphase layer becomes larger.

5.3 Compressive $M^+ \rightarrow M^-$ interphase layers ($\frac{\partial \sigma_{eq}}{\partial \theta}(\varepsilon^+, \theta^+) > 0$ and $\frac{\partial \sigma_{eq}}{\partial \theta}(\varepsilon^-, \theta^-) < 0$)

We investigate now the internal structure of traveling wave solutions for a compressive impact-induced transformation from martensitic variant M^+ to martensitic variant M^- . In this atypical case, $\frac{\partial \sigma_{eq}}{\partial \theta}$ changes its sign inside the interphase layer. We consider the front state (ε^+, θ^+) at the border between phase M^+ and the unstable region I^+ , i.e., $\varepsilon^+ = \varepsilon_m^+(\theta^+)$ (Fig. 11). Therefore, the strain–stress front state ($\varepsilon^+, \sigma^+ = \sigma_m^+(\theta^+)$) is located at the point where the isotherm $\sigma = \sigma_{eq}(\varepsilon, \theta^+)$ and the Hugoniot locus $\sigma = \sigma_H(\varepsilon; \varepsilon^+, \theta^+)$ has a local minima (Fig. 10).

Let us first consider the case of a “viscous” ($\mu > 0$), heat non-conducting traveling wave solution ($\kappa = 0$). Its trajectory in the temperature–strain plane is described by the function $\theta = \Theta_{\text{Mxw}}(\varepsilon; \varepsilon^+, \theta^+, \varepsilon^-)$. The image of this curve in the stress–strain plane, defined by relation (19), is $\sigma = \sigma_{\text{Mxw}}(\varepsilon; \varepsilon^+, \theta^+, \varepsilon^-)$, and it is plotted in Fig. 10. One can see that the chord criterion with respect to the Hugoniot locus $\sigma = \sigma_H(\varepsilon; \varepsilon^+, \theta^+)$ and the

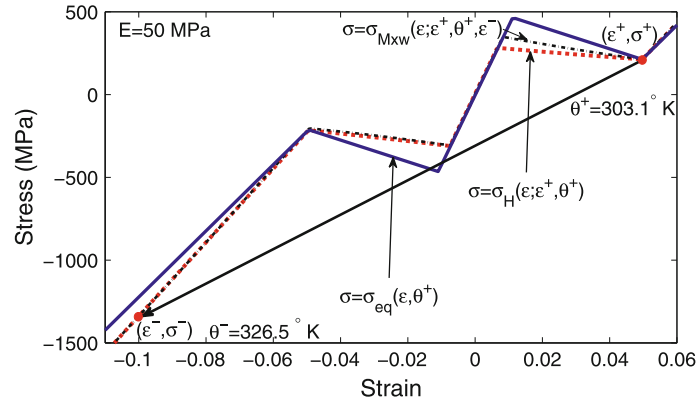


Fig. 10 Admissible compressive jump from variant M^+ to variant M^-

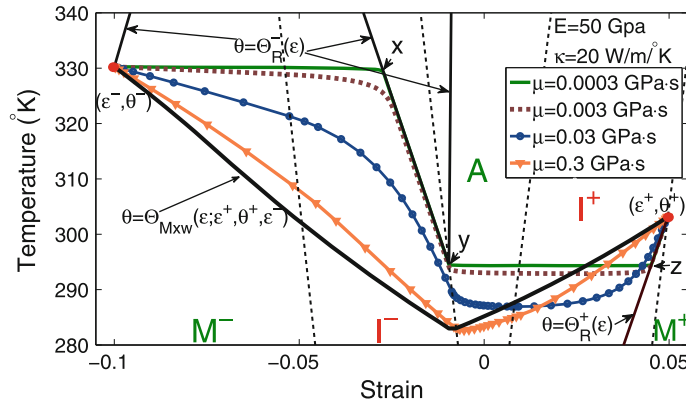


Fig. 11 Trajectories of $M^+ \rightarrow M^-$ interphase layers in the phase diagram; the explicit solutions $\theta = \Theta_R^\pm(\epsilon)$ of the implicit equation $R = 0$ given by Eq. (16); the explicit solution $\theta = \Theta_{Mxw}(\epsilon; \epsilon^+, \theta^+, \epsilon^-)$ of the implicit $H_{Mxw} = 0$ given by Eq. (17)

chord criterion with respect to the curve $\sigma = \sigma_{Mxw}(\epsilon; \epsilon^+, \theta^+, \epsilon^-)$ are both satisfied, that is, the Rayleigh line connecting the front state (ϵ^+, σ^+) and the back state (ϵ^-, σ^-) lies below both curves for $\epsilon \in (\epsilon^-, \epsilon^+)$. This condition ensures the existence and uniqueness of a $M^+ \rightarrow M^-$ interphase layer for any $\mu > 0$ and $\kappa > 0$.

Let us analyze thermomechanical aspects of the interphase layers structured only by the “viscosity.” The trajectory $\theta = \Theta_{Mxw}(\epsilon; \epsilon^+, \theta^+, \epsilon^-)$ in the phase diagram plane crosses the domains M^- , I^- and A where $\frac{\partial \sigma_{eq}}{\partial \theta} < 0$, and the domain I^+ where $\frac{\partial \sigma_{eq}}{\partial \theta} > 0$ (Fig. 11). The domains representing the phases are separated by dotted lines. As we have shown, in the general case in Part I [1, Sect 5.2.1, Case C3], this function has to be non-monotone.

Indeed, the first term in (20) is always negative since the chord criterion is fulfilled, while the second term changes its sign for $\epsilon \in (\epsilon^-, \epsilon^+)$. Indeed, it is negative when the pairs $(\tilde{\epsilon}(\epsilon), \Theta_{Mxw}(\epsilon))$ belong to phase M^- , to the unstable region I^- and to phase A , and it is positive when it belongs to the unstable region I^+ .

The numerical result shows that the curve $\theta = \Theta_{Mxw}(\epsilon; \epsilon^+, \theta^+, \epsilon^-)$ is monotonously decreasing in M^- and I^- due to the combined heating action of the internal dissipation and latent heat. Therefore, on the corresponding part of the interphase layer, the temperature has to increase for decreasing ϵ . On the other side, the curve $\theta = \Theta_{Mxw}(\epsilon; \epsilon^+, \theta^+, \epsilon^-)$ is monotonously increasing when crossing the phase domains A and I^+ . That means, according to relation (20), that the contribution of the latent heat to the cooling is larger than the contribution of the internal dissipation to the heating inside this part of the interphase layer. This implies that on the corresponding interval of the interphase layer, the temperature has to decrease for decreasing ϵ . The fact that the curve $\theta = \Theta_{Mxw}(\epsilon; \epsilon^+, \theta^+, \epsilon^-)$ is monotonously increasing when it passes through phase A where $\frac{\partial \sigma_{eq}}{\partial \theta}(\epsilon, \Theta_{Mxw}(\epsilon)) < 0$ is due to the fact that the pair $(\tilde{\epsilon}(\epsilon), \Theta_{Mxw}(\epsilon))$ defined in relation (20) belongs to I^+ , i.e., $\frac{\partial \sigma_{eq}}{\partial \theta}(\tilde{\epsilon}(\epsilon), \Theta_{Mxw}(\epsilon)) > 0$.

This non-monotone behavior of the function $\theta = \Theta_{Mxw}(\epsilon; \epsilon^+, \theta^+, \epsilon^-)$ is an expression of the fact that a continuous transformation from the variant M^+ to the variant M^- has to pass through the austenite phase A

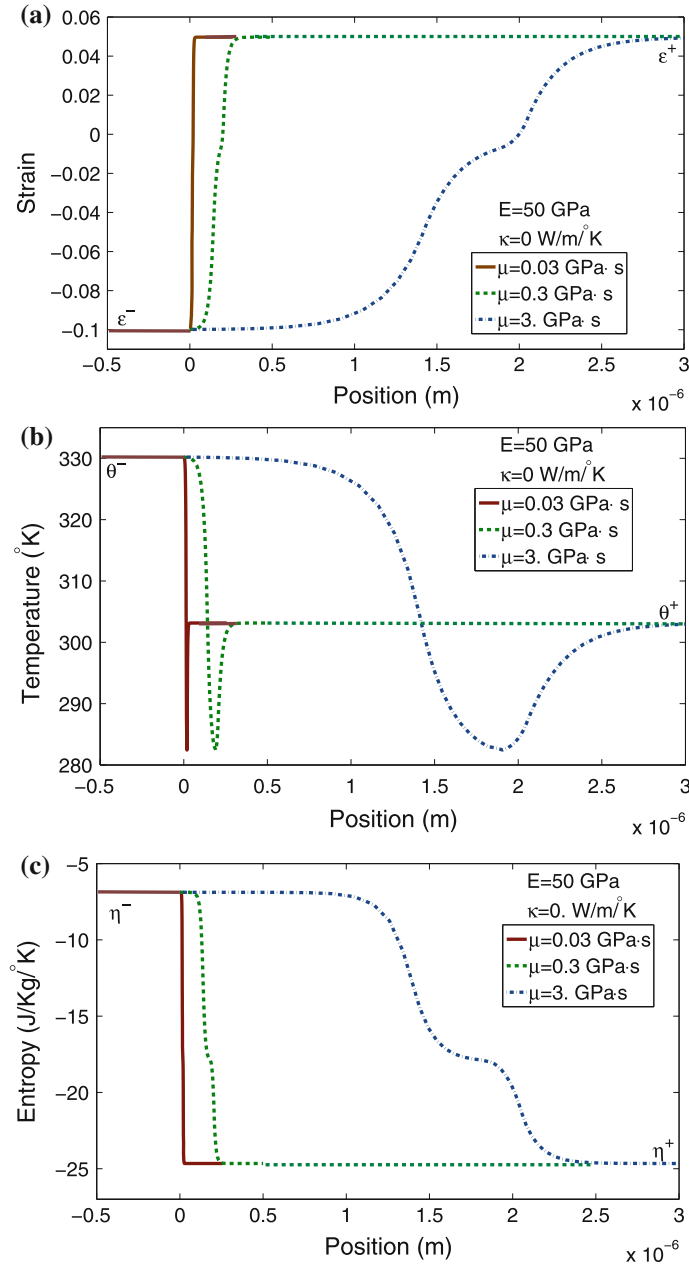


Fig. 12 **a** Strain and **b** temperature interphase layers structured only by the “viscosity” corresponding to the compressive jump in Figs. 10 and 11. **c** Monotone entropy variation inside the profile layers

and that the transformation $M^+ \rightarrow A$ is endothermic while the transformation $A \rightarrow M^-$ is exothermic. These circumstances lead to a specific structure of the temperature profile layers.

The strain, temperature, and entropy variation inside this “viscous,” heat non-conducting interphase layer is illustrated in Fig. 12. One sees that the front state temperature is 303.15 °K, the back state temperature increases to 330.2 °K, but inside the layer, there is a significant temperature drop below these two values, namely to 282.4 °K. Thus, the non-monotone variation of the temperature inside the interphase layer shows a “spike-layer” form whose width depends on the size of μ . Figure 12a, b also illustrates what happens when we consider the “viscosity” going to zero. For the strain, one gets a sharp discontinuity, but for the temperature one gets a sharp spike-layer form with two successive jumps. It is obvious that a sharp interface theory for which only the front and back states are relevant will lose this extreme value of the temperature profile. In

other words, an important physical aspect related to an impact-induced phase transformation from martensitic variant M^+ to martensitic variant M^- will be disregarded, that is, the passage of the particles through the austenite phase A .

Concerning the entropy variation inside the interphase layers structured only by “viscosity,” we get, as expected (see Part I [1, Sect. 5.2.3], a monotone variation (Fig. 12c).

Let us analyze the case when both the “viscosity” and the heat conduction are structuring mechanisms of the interphase layer. When the heat conductivity has the fixed value $\kappa = 20 \text{ W/m}^\circ\text{K}$ and the “viscosity” has values increasingly smaller, then the graphic of the function $\theta = \Theta(\varepsilon; \mu, \kappa)$, for $\varepsilon \in (\varepsilon^-, \varepsilon^+)$, is illustrated in Fig. 11. For each μ , this function is non-monotone and has a minimum below the front and back state temperatures θ^\pm . This minimum value of the temperature increases as μ decreases, i.e., as the role of the “viscosity” becomes more and more insignificant with respect to the heat conductivity effect.

The structure of strain and temperature interphase layer for “viscosities” ranging from $\mu = 3 \text{ GPa s}$ (“viscosity” structuring effect is dominant with respect to the heat conductivity effect) to $\mu = 0.0003 \text{ GPa s}$ (“viscosity” structuring effect is completely negligible with respect to the heat conductivity effect) is illustrated in Figs. 13 and 14. The temperature variation inside the interphase layer is again non-monotone and has a *spike-layer form* reflecting the manifestation of the *endothermic* character of the $M^+ \rightarrow A$ transformation and the *exothermic* character of the $A \rightarrow M^-$ phase transformation. The minimum value of the temperature reached inside the layer varies from $282.3 \text{ }^\circ\text{K}$ for $\mu = 3 \text{ GPa s}$ to $294.3 \text{ }^\circ\text{K}$ (temperature corresponding to YZ line in Fig. 11) for $\mu = 0.0003 \text{ GPa s}$. This latter case can be practically assimilated with the case when the only structuring mechanism of the profile layer is the heat conduction.

Figure 11 also illustrates that the Rayleigh set $\{(\varepsilon, \theta) | R(\varepsilon, \theta) = 0\}$ in the $\varepsilon - \theta$ phase diagram is composed by two disconnected piecewise linear curves $\theta = \Theta_R^\pm(\varepsilon)$, one passing trough $(\varepsilon^+, \theta^+)$ and the other trough $(\varepsilon^-, \theta^-)$, as a consequence of the fact that $\frac{\partial \sigma_{eq}}{\partial \theta}$ has different signs at the front and back state. On the other side, Fig. 11 shows how for fixed κ and $\mu \rightarrow 0$ the trajectories $\theta = \Theta(\varepsilon; \mu, \kappa)$ are increasingly close to some parts of the Rayleigh set in the $\varepsilon - \theta$ plane and how the solution of the reduced system (24) is approached.

For $\mu = 0.0003 \text{ GPa s}$ the trajectory is composed by a nearly horizontal line starting at the back state $(\varepsilon^-, \theta^-)$, passing very close to a point $X = (\varepsilon_x, \theta_x)$ which belongs to the branch $\theta = \Theta_R^-(\varepsilon)$ of the Rayleigh set, i.e., $\Theta_R^-(\varepsilon_x) = \theta^-$, is followed by a curve that matches the curve $\theta = \Theta_R^-(\varepsilon)$ until near its minimum point $Y = (\varepsilon_y, \theta_y = \Theta_R^-(\varepsilon_y))$, next is followed by another nearly horizontal line which connects the point Y with the point $Z = (\varepsilon_z, \theta_z = \Theta_R^+(\varepsilon_z))$, belonging to the branch $\theta = \Theta_R^+(\varepsilon)$ of the Rayleigh set, and finally is followed by a curve which matches $\theta = \Theta_R^+(\varepsilon)$ and ends at the point $(\varepsilon^+, \theta^+)$. This behavior is justified in Part I [1, Sect 5.2.1 Case C3].

This limit case shows that when the only structuring mechanism is the heat conduction, the strain profile contains isothermal jumps in strain from ε^- to ε_x and from ε_y to ε_z as it is illustrated in Fig. 14a. One observes that we have a smooth variation of the strain profile only when the trajectory of the “non-viscous,” heat conducting traveling wave solution sweeps parts of the Rayleigh set in the $\varepsilon - \theta$ plane. The temperature profile is continuous and has a minimum corresponding to the temperature at the point $Y = (\varepsilon_y, \theta_y)$ in Fig. 11.

Figures 13c and 14c show how the entropy variation inside the profile layer turns from a monotone behavior to a non-monotone behavior as the role of the heat conduction increases at the expense of the role of the “viscosity” as structuring mechanisms. Moreover, the entropy inside the profile layer can become considerably smaller than its value at the front state η^+ and considerably larger than its value at the Hugoniot back state $\eta^- > \eta^+$. This behavior is known as the phenomenon of entropy undershoot and entropy overshoot, respectively. The limiting case $\mu = 0.0003 \text{ GPa s}$ in Fig. 14c also illustrates that in a “non-viscous,” heat conducting profile layer, i.e., when the only structuring mechanism is the heat conduction, the entropy profile contains isothermal jumps in entropy.

This example clearly illustrates the profound difference in the effect of “viscosity” (time of relaxation) and the effect of heat conduction on the structure of transition layers.

Our numerical investigation also offers some insight into the width of the interphase layers. A correspondence between the time of relaxation (“viscosity”) and the thickness of the transition layers is illustrated in Table 5. As expected, one observes that the width of the profile layer increases as the time of relaxation increases. Indeed, when the dominant structuring mechanism is the heat conduction ($\mu = 0.0003 \text{ GPa s}$), then the width of the transition layer is of the order of hundredths of micrometers (or, tens of nanometers) while when the “viscosity” effect is dominant ($\mu = 30 \text{ GPa s}$), the width is of the order of hundreds of micrometers.

Since the heat conduction can be determined independently from laboratory experiments, the identification of the time of relaxation remains an open problem.

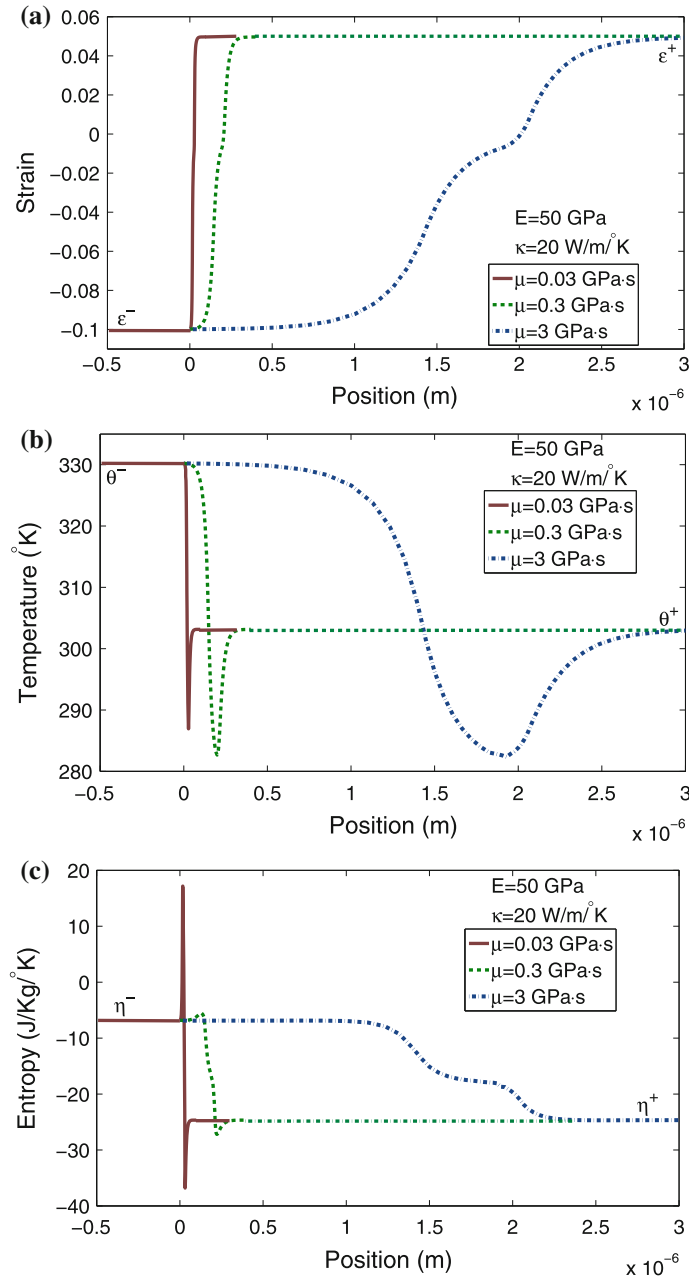


Fig. 13 Evolution of the **a** strain and **b** temperature profile layers corresponding to the compressive jump in Figs. 10 and 11 when the “viscosity” structuring effect diminishes at the expense of the heat conductivity structuring effect. **c** Transition from monotone to non-monotone entropy variation inside the profile layers

It is useful to recall that the value of the time of relaxation which has been used in numerical simulations of quasi-static strain-controlled experiments in Făciu and Mihăilescu-Sulciu [22] and which showed a good agreement with laboratory tests performed by Shaw and Kyriakides [27] was $\tau = 10^{-4}$ s. The numerical experiments have put into evidence the capability of the Maxwellian rate-type approach to describe the mechanism of phase transformation that occurs via nucleation and growth of phases as a consequence of instability phenomena. Moreover, we found that, for the values of τ lower than 10^{-5} s, which enhances the mechanisms of thermomechanical instability in the spinodal region, or for values of τ larger than 10^{-2} s, which weakens the instability phenomena, one gets inaccurate predictions. Therefore, if we consider the proper values for the time of relaxation τ in the range of 10^{-4} and 10^{-3} s, one gets that the width of a propagating interphase layer,

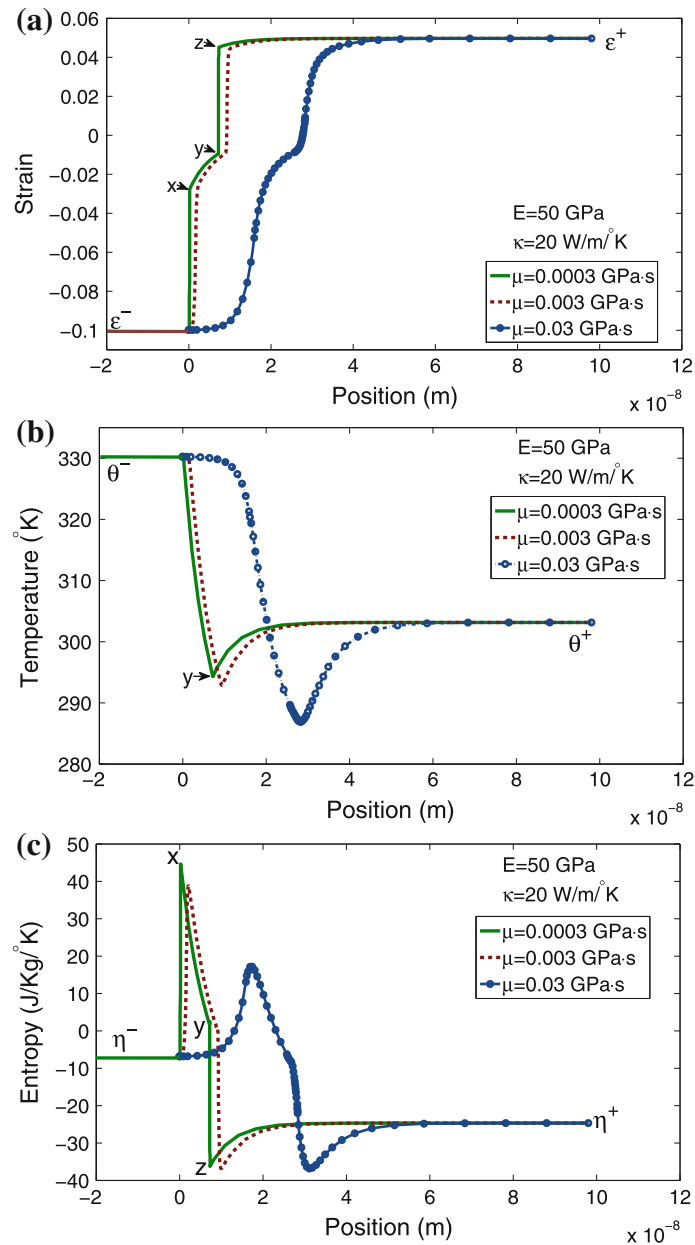


Fig. 14 Evolution of the **a** strain and **b** temperature profile layers corresponding to the compressive jump in Figs. 10 and 11 when the conductivity structuring effect largely dominates the “viscosity” structuring effect. **c** Non-monotone entropy variation inside the profile layers—entropy “overshoot” and entropy “undershoot” phenomena

structured by the time of relaxation and an usual value of the heat conduction for an SMA, is also of the order of hundredths of micrometers.

6 Conclusions

The transition across a propagating interface separating two phases of a material cannot be instantaneous. Therefore, a transition layer should exist. We have modeled the internal structure of this interphase layer by introducing dissipative mechanisms in the form of Maxwellian rate-type effects and heat conduction. The main aspects of the response of an SMA have been described by using the thermoelasticity theory with non-monotone stress–strain relation. A piecewise linear thermoelastic relation has been fitted with laboratory experiments in

Table 5 Order of magnitude of the width of a profile layer for different values of the “viscosity” parameter μ when $E = 50$ GPa and $\kappa = 20$ W/m $^\circ$ K

| “viscosity” μ | 0.0003 GPa s | 0.003 GPa s | 0.03 GPa s | 0.3 GPa s | 3 GPa s | 30 GPa s |
|---|--------------------|--------------------|--------------------|--------------------|--------------------|--------------------|
| Time of relaxation $\tau = \frac{\mu}{E}$ (s) | 6×10^{-6} | 6×10^{-5} | 6×10^{-4} | 6×10^{-3} | 6×10^{-2} | 6×10^{-1} |
| Interphase width (μm) | ≈ 0.02 | ≈ 0.04 | ≈ 0.05 | ≈ 0.25 | ≈ 2 | ≈ 30 |

such a way that the variation with respect to the temperature of the local maxima and minima of the stress–strain relations matches the rate of increase of the hysteresis stress plateau with respect to the temperature in traction tests. This approach allowed us to capture in an accurate way the effect of the latent heat in phase transformation processes.

In studying impact-induced phase transition phenomena, one should focus both from theoretical and experimental point of view on the investigation of thermal aspects. Indeed, our quantitative analysis has put into evidence that in an SMA, there are large temperature variations across a propagating interphase separating two phases of the material (more than 20 $^\circ$ K) even if its speed is very low. Therefore, such significant temperature changes should be exploited from the experimental point of view because they are an extremely valuable indication of a dynamic phase transformation process. We emphasized the influence of the internal dissipation and of the latent heat on the structure of the interphase layers. Thus, we showed how compressive moving phase boundaries $A \rightarrow M^-$ are of heating type and how the reverse expansive moving phase boundaries from $M^- \rightarrow A$ are of cooling type, capturing in this way the influence of the exothermic and endothermic character of phase transitions. We pointed out that across a propagating interphase layer separating the two variants of martensite, M^+ and M^- , the temperature suffers large variation (about 23 $^\circ$ K), but the most striking aspect revealed is that there are places inside the profile layers where some particles experience temperatures considerably lower than that at its front state and its back state. We also note that a sharp interface theory cannot predict this spike-layer form of the temperature. This phenomenon of temperature undershoot, if it could be detected experimentally, can be a direct proof of the existence of an internal structure of a propagating phase boundary. The experimental detection through infrared radiation of a moving interface separating different phases of a material, and even more of a phenomenon of temperature undershoot/overshoot is a challenge which depends on the development of highly accurate temperature measurement instruments with high acquisition data.

On the other side, it is reasonable to interpret a propagating interphase layer as a sharp phase boundary if its thickness is small compared to other dimensions of interest. Therefore, in many practical impact experiments, the solutions can be constructed by using the adiabatic thermoelastic system endowed with an admissibility criterion to select physical relevant jump discontinuities. The chord criterion with respect to the Hugoniot locus can be considered by some authors, who have used the effects of both “viscosity” and strain-gradient effects (Slemrod [17], Ngan and Truskinovsky [20,21]), as too restrictive since it rules out propagating phase boundaries near the equilibrium coexistence line, named also subsonic phase boundaries or kinks. On the other side, according to Vainchtein [16] (see also Vainchtein and Rosakis [31] and Vainchtein [32]), models which include strain-gradient effects cannot capture realistic hysteresis loops under quasi-static (isothermal) strain rate–controlled loading conditions. Since different selection criteria may furnish different solutions to a Riemann problem, only systematic impact experiments as for example those performed by Escobar and Clifton (1995) could decide which is the physically relevant one.

Acknowledgements The authors are grateful to the reviewers for their useful observations. C. F. acknowledges support from the Romanian Ministry of Education and Research through Project PCCE ID_100/2010. A. M. acknowledges support from Laboratoire Européen Associé CNRS Franco-Roumain Mathématiques & Modélisation.

Appendix A: The thermodynamic potentials for the thermoelastic model

The stress response function defined by relations (1)–(3) becomes

$$\sigma = \sigma_{eq}(\varepsilon, \theta) = \begin{cases} E_3\varepsilon - (\alpha E_3 + a)\theta + \alpha E_3\theta_T + b, & \text{for } \varepsilon \leq \varepsilon_m^-(\theta) \\ -E_2\varepsilon + (\alpha E_2 - d)\theta - \alpha E_2\theta_T + d\theta_m, & \text{for } \varepsilon_m^-(\theta) < \varepsilon < \varepsilon_M^-(\theta) \\ E_1\varepsilon - \alpha E_1(\theta - \theta_T), & \text{for } \varepsilon_M^-(\theta) \leq \varepsilon \leq \varepsilon_M^+(\theta) \\ -E_2\varepsilon + (\alpha E_2 + d)\theta - \alpha E_2\theta_T - d\theta_m, & \text{for } \varepsilon_M^+(\theta) < \varepsilon < \varepsilon_m^+(\theta) \\ E_3\varepsilon - (\alpha E_3 - a)\theta + \alpha E_3\theta_T - b, & \text{for } \varepsilon_m^+(\theta) \leq \varepsilon \end{cases} \quad (22)$$

where

$$a = M(E_1 + E_2) - m(E_2 + E_3), \quad b = (E_1 - E_3)M\theta_m + (E_2 + E_3)(M - m)\theta_M, \quad d = M(E_1 + E_2). \quad (23)$$

The free energy $\psi = \psi_{eq}(\varepsilon, \theta)$, the entropy $\eta = \eta_{eq}(\varepsilon, \theta)$ and the specific heat at constant strain $C_{eq}(\varepsilon, \theta)$ of the thermoelastic model are uniquely determined by the stress response function (modulo an additive function of temperature) according to relations $\sigma_{eq}(\varepsilon, \theta) = \rho \frac{\partial \psi_{eq}(\varepsilon, \theta)}{\partial \varepsilon}$, $\eta_{eq}(\varepsilon, \theta) = -\frac{\partial \psi_{eq}}{\partial \theta}(\varepsilon, \theta)$, and $C_{eq}(\varepsilon, \theta) = -\theta \frac{\partial^2 \psi_{eq}(\varepsilon, \theta)}{\partial \theta^2}$ at the points where the derivatives make sense.

If $\sigma = \sigma_{eq}(\varepsilon, \theta)$ is only continuous and piecewise smooth like in (1)–(3), then the free energy $\rho\psi_{eq}(\varepsilon, \theta) = \rho\phi(\theta) + \int_{\varepsilon_0}^{\varepsilon} \sigma_{eq}(s, \theta) ds$ is of class C^1 , the entropy $\rho\eta_{eq}(\varepsilon, \theta) = -\rho\phi'(\theta) - \int_{\varepsilon_0}^{\varepsilon} \frac{\partial \sigma_{eq}(s, \theta)}{\partial \theta} ds$ as well as the internal energy $e = e_{eq}(\varepsilon, \theta) = \psi_{eq} + \theta\eta_{eq}$ are of class C^0 . Here, prime denotes the derivative.

The specific heat $C = C_{eq}(\varepsilon, \theta)$ is a discontinuous function on its domain of definition. Indeed, let us recall the following result. If $f = f(\varepsilon, \theta)$ is continuous and continuously differentiable with respect to θ except for a single discontinuity whose position is given by a differentiable function $\varepsilon = \varepsilon^*(\theta) \in (\varepsilon_1, \varepsilon_2)$, then we have

$$\frac{d}{d\theta} \int_{\varepsilon_1}^{\varepsilon_2} f(\varepsilon, \theta) d\varepsilon = \int_{\varepsilon_1}^{\varepsilon_2} \frac{\partial f(\varepsilon, \theta)}{\partial \theta} d\varepsilon - \frac{d\varepsilon^*(\theta)}{d\theta} \llbracket f \rrbracket(\varepsilon^*(\theta), \theta) \quad (24)$$

where $\llbracket f \rrbracket(\varepsilon^*(\theta), \theta) = f(\varepsilon^*(\theta) + 0, \theta) - f(\varepsilon^*(\theta) - 0, \theta)$ and $f(\varepsilon^*(\theta) \pm 0, \theta)$ denote the one-sided limits of $f(\varepsilon, \theta)$ as ε approaches $\varepsilon^*(\theta)$ from the right and from the left.

Let us take $\varepsilon_0 = \varepsilon_M^{\pm}(\theta_m) = \alpha(\theta_m - \theta_T)$ the only strain which always lies between $\varepsilon_M^-(\theta)$ and $\varepsilon_M^+(\theta)$. Then, when $\frac{\partial \sigma}{\partial \theta}$ is discontinuous across the curves $\varepsilon = \varepsilon_M^{\pm}(\theta)$ and $\varepsilon = \varepsilon_m^{\pm}(\theta)$ by using (24), one derives the specific heat as

$$C_{eq}(\varepsilon, \theta) = -\theta \int_{\varepsilon_0}^{\varepsilon} \frac{1}{\rho} \frac{\partial^2 \sigma_{eq}(s, \theta)}{\partial \theta^2} ds - \theta \phi''(\theta) + \frac{\theta}{\rho} \begin{cases} -\frac{d\varepsilon_M^-(\theta)}{d\theta} \llbracket \frac{\partial \sigma_{eq}}{\partial \theta} \rrbracket(\varepsilon_M^-(\theta), \theta) - \frac{d\varepsilon_m^-(\theta)}{d\theta} \llbracket \frac{\partial \sigma_{eq}}{\partial \theta} \rrbracket(\varepsilon_m^-(\theta), \theta), & \text{for } \varepsilon < \varepsilon_m^+(\theta) \\ -\frac{d\varepsilon_M^-(\theta)}{d\theta} \llbracket \frac{\partial \sigma_{eq}}{\partial \theta} \rrbracket(\varepsilon_M^-(\theta), \theta), & \text{for } \varepsilon_m^-(\theta) < \varepsilon < \varepsilon_M^-(\theta) \\ 0 & \text{for } \varepsilon_M^-(\theta) < \varepsilon < \varepsilon_M^+(\theta) \\ \frac{d\varepsilon_M^+(\theta)}{d\theta} \llbracket \frac{\partial \sigma_{eq}}{\partial \theta} \rrbracket(\varepsilon_M^+(\theta), \theta), & \text{for } \varepsilon_M^+(\theta) < \varepsilon < \varepsilon_m^+(\theta) \\ \frac{d\varepsilon_M^+(\theta)}{d\theta} \llbracket \frac{\partial \sigma_{eq}}{\partial \theta} \rrbracket(\varepsilon_M^+(\theta), \theta) + \frac{d\varepsilon_m^+(\theta)}{d\theta} \llbracket \frac{\partial \sigma_{eq}}{\partial \theta} \rrbracket(\varepsilon_m^+(\theta), \theta), & \text{for } \varepsilon_m^+(\theta) < \varepsilon \end{cases} \quad (25)$$

where $\phi(\theta)$ is determined according to relation

$$-\theta \phi''(\theta) = C_{eq}(\varepsilon_0, \theta). \quad (26)$$

Relation (26) expresses the fact that it is sufficient to know experimentally the specific heat at the constant strain ε_0 for an interval of temperature in order to determine function $\phi = \phi(\theta)$.

Assuming that the specific heat in the austenitic phase is constant, i.e., $C(\varepsilon_0, \theta) = C > 0$, one gets from relation (26) that

$$\phi(\theta) = -C\theta \ln \frac{\theta}{\theta_T} + C(\theta - \theta_T), \quad (27)$$

where we have assumed that $\psi_{eq}(\varepsilon_0, \theta_T) = 0$ and $\eta_{eq}(\varepsilon_0, \theta_T) = 0$.

The specific heat for the thermoelastic model (1)–(3) is then given by

$$\rho C_{eq}(\varepsilon, \theta) = \rho C + \theta \begin{cases} (E_1 + E_2)(\alpha - M)^2 - (E_2 + E_3)(\alpha - m)^2, & \text{if } \varepsilon \leq \varepsilon_m^-(\theta) \\ (E_1 + E_2)(\alpha - M)^2, & \text{if } \varepsilon_m^-(\theta) < \varepsilon < \varepsilon_M^-(\theta) \\ 0, & \text{if } \varepsilon_M^-(\theta) \leq \varepsilon \leq \varepsilon_M^+(\theta) \\ (E_1 + E_2)(\alpha + M)^2, & \text{if } \varepsilon_M^+(\theta) < \varepsilon < \varepsilon_m^+(\theta) \\ (E_1 + E_2)(\alpha + M)^2 - (E_2 + E_3)(\alpha + m)^2, & \text{if } \varepsilon_m^+(\theta) \leq \varepsilon \end{cases}. \quad (28)$$

The free energy and the internal energy are, respectively, given by

$$\rho\psi_{eq}(\varepsilon, \theta) = \rho\phi(\theta) + \alpha E_1 \varepsilon_0 (\theta - \theta_T) - \frac{E_1}{2} \varepsilon_0^2$$

$$+ \begin{cases} \frac{E_3}{2} \varepsilon^2 + (\sigma_m^-(\theta) - E_3 \varepsilon_m^-(\theta)) \varepsilon + \frac{E_2 + E_3}{2} (\varepsilon_m^-(\theta))^2 - \frac{E_1 + E_2}{2} (\varepsilon_M^-(\theta))^2, & \text{if } \varepsilon \leq \varepsilon_m^-(\theta) \\ -\frac{E_2}{2} \varepsilon^2 + (\sigma_M^-(\theta) + E_2 \varepsilon_M^-(\theta)) \varepsilon - \frac{E_1 + E_2}{2} (\varepsilon_M^-(\theta))^2, & \text{if } \varepsilon_m^-(\theta) < \varepsilon < \varepsilon_M^-(\theta) \\ \frac{E_1}{2} \varepsilon^2 - \alpha E_1 (\theta - \theta_T) \varepsilon, & \text{if } \varepsilon_M^-(\theta) \leq \varepsilon \leq \varepsilon_M^+(\theta) \\ -\frac{E_2}{2} \varepsilon^2 + (\sigma_M^+(\theta) + E_2 \varepsilon_M^+(\theta)) \varepsilon - \frac{E_1 + E_2}{2} (\varepsilon_M^+(\theta))^2, & \text{if } \varepsilon_M^+(\theta) < \varepsilon < \varepsilon_m^+(\theta) \\ \frac{E_3}{2} \varepsilon^2 + (\sigma_m^+(\theta) - E_3 \varepsilon_m^+(\theta)) \varepsilon + \frac{E_2 + E_3}{2} (\varepsilon_m^+(\theta))^2 - \frac{E_1 + E_2}{2} (\varepsilon_M^+(\theta))^2, & \text{if } \varepsilon_m^+(\theta) \leq \varepsilon \end{cases}, \quad (29)$$

$$\rho e_{eq}(\varepsilon, \theta) = \rho C (\theta - \theta_T) - \alpha E_1 \varepsilon_0 \theta_T - \frac{E_1}{2} \varepsilon_0^2$$

$$+ \begin{cases} \frac{E_3}{2} \varepsilon^2 + (\alpha E_3 \theta_T + b) \varepsilon + A^- \theta^2 + B^-, & \text{if } \varepsilon \leq \varepsilon_m^-(\theta) \\ -\frac{E_2}{2} \varepsilon^2 - (\alpha E_2 \theta_T - d \theta_m) \varepsilon + D^- \theta^2 + F^-, & \text{if } \varepsilon_m^-(\theta) < \varepsilon < \varepsilon_M^-(\theta) \\ \frac{E_1}{2} \varepsilon^2 + \alpha E_1 \theta_T \varepsilon, & \text{if } \varepsilon_M^-(\theta) \leq \varepsilon \leq \varepsilon_M^+(\theta) \\ -\frac{E_2}{2} \varepsilon^2 - (\alpha E_2 \theta_T + d \theta_m) \varepsilon + D^+ \theta^2 + F^+, & \text{if } \varepsilon_M^+(\theta) < \varepsilon < \varepsilon_m^+(\theta) \\ \frac{E_3}{2} \varepsilon^2 + (\alpha E_3 \theta_T - b) \varepsilon + A^+ \theta^2 + B^+, & \text{if } \varepsilon_m^+(\theta) \leq \varepsilon \end{cases} \quad (30)$$

where

$$D^\pm = \frac{E_1 + E_2}{2} (\alpha \pm M)^2, \quad F^\pm = -\frac{E_1 + E_2}{2} (\alpha \theta_T \pm M \theta_m)^2, \quad (31)$$

$$A^\pm = D^\pm - \frac{E_2 + E_3}{2} (\alpha \pm m)^2, \quad B^\pm = F^\pm + \frac{E_2 + E_3}{2} (\alpha \theta_T \mp (M - m) \theta_M \pm M \theta_m)^2.$$

Appendix B: The thermodynamic potentials for the Maxwellian rate-type model

We consider the Maxwellian rate-type constitutive equation (9) having the equilibrium described by the piecewise linear stress–strain–temperature relation (1)–(3). According to (10), the free energy function is given by

$$\rho\psi_{Mxw}(\varepsilon, \sigma, \theta) = \frac{1}{2E} \sigma^2 + \varphi_1(\theta)$$

$$+ \begin{cases} \frac{E_3}{2E(E-E_3)} (\sigma - E\varepsilon)^2 + \left(\frac{\alpha E_3 - a}{E-E_3} \theta - \frac{\alpha E_3 \theta_T - b}{E-E_3} \right) (\sigma - E\varepsilon) + \varphi_3^+(\theta), & \text{if } \sigma - E\varepsilon \leq \tau_m^+(\theta), \\ -\frac{E_2}{2E(E+E_2)} (\sigma - E\varepsilon)^2 - \left(\frac{\alpha E_2 + d}{E+E_2} \theta - \frac{\alpha E_2 \theta_T + d \theta_m}{E+E_2} \right) (\sigma - E\varepsilon) + \varphi_2^+(\theta), & \text{if } \tau_m^+(\theta) < \sigma - E\varepsilon < \tau_M^+(\theta), \\ \frac{E_1}{2E(E-E_1)} (\sigma - E\varepsilon)^2 + \frac{E_1 \alpha}{E-E_1} (\theta - \theta_T) (\sigma - E\varepsilon), & \text{if } \tau_M^+(\theta) \leq \sigma - E\varepsilon \leq \tau_M^-(\theta), \\ -\frac{E_2}{2E(E+E_2)} (\sigma - E\varepsilon)^2 - \left(\frac{\alpha E_2 - d}{E+E_2} \theta - \frac{\alpha E_2 \theta_T - d \theta_m}{E+E_2} \right) (\sigma - E\varepsilon) + \varphi_2^-(\theta), & \text{if } \tau_M^-(\theta) < \sigma - E\varepsilon < \tau_m^-(\theta), \\ \frac{E_3}{2E(E-E_3)} (\sigma - E\varepsilon)^2 + \left(\frac{\alpha E_3 + a}{E-E_3} \theta - \frac{\alpha E_3 \theta_T + b}{E-E_3} \right) (\sigma - E\varepsilon) + \varphi_3^-(\theta), & \text{if } \tau_m^-(\theta) \leq \sigma - E\varepsilon, \end{cases} \quad (32)$$

where

$$\varphi_1(\theta) = \frac{E_1^2 \alpha^2}{2(E-E_1)} (\theta - \theta_T)^2 - \rho C \theta \ln \frac{\theta}{\theta_T} + (\rho C + \alpha E_1 \varepsilon_0) (\theta - \theta_T) - \frac{E_1}{2} \varepsilon_0^2, \quad (33)$$

$$\varphi_2^\pm(\theta) = -\frac{(E_1 + E_2)}{2(E + E_2)(E - E_1)} (\tau_M^\pm(\theta))^2, \quad \varphi_3^\pm(\theta) = \varphi_2^\pm(\theta) + \frac{(E_3 + E_2)}{2(E + E_2)(E - E_3)} (\tau_m^\pm(\theta))^2,$$

and, by using notation $h(\varepsilon, \theta) = \sigma_{eq}(\varepsilon, \theta) - E\varepsilon$,

$$\tau_M^\pm(\theta) = h(\varepsilon_M^\pm(\theta), \theta) = -E\alpha(\theta - \theta_T) \mp M(E - E_1)(\theta - \theta_m),$$

$$\tau_m^\pm(\theta) = h(\varepsilon_m^\pm(\theta), \theta) = -E\alpha(\theta - \theta_T) \pm (M - m)(E + E_2)(\theta - \theta_M) \mp M(E - E_1)(\theta - \theta_m).$$

Assuming that the additive function of temperature $\phi = \phi(\theta)$ in the definition of the free energy function of the Maxwellian model (10) is the same with the additive function of temperature in the definition of the free energy of the associated thermoelastic model, we have shown in Part I [1] that at equilibrium the following relation $\rho C_{\text{Mxw}}(\varepsilon, \sigma_{eq}(\varepsilon, \theta), \theta) = \rho C_{eq}(\varepsilon, \theta) - \theta \left(\frac{\partial \sigma_{eq}}{\partial \theta} \right)^2 / \left(E - \frac{\partial \sigma_{eq}}{\partial \varepsilon} \right)$ holds. Therefore, according to relations (26), (27), we have $\rho C_{\text{Mxw}}(\varepsilon_0, \sigma_{eq}(\varepsilon_0, \theta), \theta) = \rho C - \theta (E_1 \alpha)^2 / (E - E_1)$, where $\varepsilon_0 = \varepsilon_M^\pm(\theta_m) = \alpha(\theta_m - \theta_T)$. Moreover, the free energy and the entropy at the reference equilibrium state are zero, i.e., $\psi_{\text{Mxw}}(\varepsilon_0, \sigma_{eq}(\varepsilon_0, \theta_T), \theta_T) = \psi_{eq}(\varepsilon_0, \theta_T) = 0$ and $\eta_{\text{Mxw}}(\varepsilon_0, \sigma_{eq}(\varepsilon_0, \theta_T), \theta_T) = \eta_{eq}(\varepsilon_0, \theta_T) = 0$. Thus, the specific heat of the Maxwellian model is given by

$$\rho C_{\text{Mxw}}(\varepsilon, \sigma, \theta) = \rho C - \frac{E_1^2 \alpha^2}{(E - E_1)} \theta + \theta \begin{cases} 2A_{\text{Mxw}}^+, & \text{if } \sigma - E\varepsilon \leq \tau_m^+(\theta), \\ 2D_{\text{Mxw}}^+, & \text{if } \tau_m^+(\theta) < \sigma - E\varepsilon < \tau_M^+(\theta), \\ 0, & \text{if } \tau_M^+(\theta) \leq \sigma - E\varepsilon \leq \tau_M^-(\theta), \\ 2D_{\text{Mxw}}^-, & \text{if } \tau_M^-(\theta) < \sigma - E\varepsilon < \tau_m^-(\theta), \\ 2A_{\text{Mxw}}^-, & \text{if } \tau_m^-(\theta) \leq \sigma - E\varepsilon, \end{cases}$$

and the internal energy by

$$\rho e_{\text{Mxw}}(\varepsilon, \sigma, \theta) = \rho C(\theta - \theta_T) - \alpha E_1 \varepsilon_0 \theta_T - \frac{E_1}{2} \varepsilon_0^2 - \frac{E_1^2 \alpha^2}{2(E - E_1)} (\theta^2 - \theta_T^2) + \frac{1}{2E} \sigma^2, \\ + \begin{cases} \frac{E_3}{2E(E-E_3)} (\sigma - E\varepsilon)^2 - \frac{\alpha E_3 \theta_T - b}{E-E_3} (\sigma - E\varepsilon) + A_{\text{Mxw}}^+ \theta^2 + B_{\text{Mxw}}^+, & \text{if } \sigma - E\varepsilon \leq \tau_m^+(\theta), \\ -\frac{E_2}{2E(E+E_2)} (\sigma - E\varepsilon)^2 + \frac{\alpha E_2 \theta_T + d \theta_m}{E+E_2} (\sigma - E\varepsilon) + D_{\text{Mxw}}^+ \theta^2 + F_{\text{Mxw}}^+, & \text{if } \tau_m^+(\theta) < \sigma - E\varepsilon < \tau_M^+(\theta), \\ \frac{E_1}{2E(E-E_1)} (\sigma - E\varepsilon)^2 - \frac{E_1 \alpha \theta_T}{E-E_1} (\sigma - E\varepsilon), & \text{if } \tau_M^+(\theta) \leq \sigma - E\varepsilon \leq \tau_M^-(\theta), \\ -\frac{E_2}{2E(E+E_2)} (\sigma - E\varepsilon)^2 + \frac{\alpha E_2 \theta_T - d \theta_m}{E+E_2} (\sigma - E\varepsilon) + D_{\text{Mxw}}^- \theta^2 + F_{\text{Mxw}}^-, & \text{if } \tau_M^-(\theta) < \sigma - E\varepsilon < \tau_m^-(\theta), \\ \frac{E_3}{2E(E-E_3)} (\sigma - E\varepsilon)^2 - \frac{\alpha E_3 \theta_T + b}{E-E_3} (\sigma - E\varepsilon) + A_{\text{Mxw}}^- \theta^2 + B_{\text{Mxw}}^-, & \text{if } \tau_m^-(\theta) \leq \sigma - E\varepsilon, \end{cases} \quad (34)$$

where

$$D_{\text{Mxw}}^\pm = \frac{(E_1 + E_2)(E\alpha \pm M(E - E_1))^2}{2(E + E_2)(E - E_1)}, \quad F_{\text{Mxw}}^\pm = -\frac{(E_1 + E_2)(E\alpha \theta_T \pm M(E - E_1)\theta_m)^2}{2(E + E_2)(E - E_1)}, \\ A_{\text{Mxw}}^\pm = D_{\text{Mxw}}^\pm - \frac{(E_3 + E_2)(E\alpha \pm M(E - E_1) \mp (M - m)(E + E_2))^2}{2(E + E_2)(E - E_3)}, \quad (35) \\ B_{\text{Mxw}}^\pm = F_{\text{Mxw}}^\pm + \frac{(E_3 + E_2)(E\alpha \theta_T \pm M(E - E_1)\theta_m \mp (M - m)(E + E_2)\theta_m)^2}{2(E + E_2)(E - E_3)}.$$

References

1. Făciu, C., Molinari, A.: The structure of shock and interphase layers for a heat conducting Maxwellian rate-type approach to solid–solid phase transitions. Part I: Thermodynamics and admissibility. *Acta Mech.* doi: [10.1007/s00707-013-0846-x](https://doi.org/10.1007/s00707-013-0846-x)
2. Barker, L.M.: Fine structure of compression and release wave shapes in aluminium measured by velocity interferometer technique. In: Berger, J. (ed.) *Behavior of Dense Media Under High Dynamic Pressures*, pp. 483–504. Gordon and Breach, New York (1968)
3. Molinari, A., Ravichandran, G.: Fundamental structure of steady plastic shock waves in metals. *J. Appl. Phys.* **95**, 1718–1732 (2004)
4. Grady, D.E.: Structured shock waves and the fourth-power law. *J. Appl. Phys.* **107**, 013506(1–13) (2010)
5. Escobar, J.C., Clifton, R.J.: On pressure-shear plate impact for studying the kinetics of stress-induced phase transformations. *Mater. Sci. Eng. Solids A* **179**, 125–142 (1993)
6. Făciu, C., Molinari, A.: On the longitudinal impact of two phase transforming bars. Elastic versus a rate-type approach. Part I: The elastic case. Part II: The rate-type case. *Int. J. Solids Struct.* **43**, 497–522 and 523–550 (2006)
7. Erskine, D.J., Nellis, W.J.: Shock-induced martensitic transformation of highly oriented graphite to diamond. *J. Appl. Phys.* **71**, 4882–4886 (1992)
8. Lagoudas, D.C., Ravi-Chandar, K., Sarh, K., Popov, P.: Dynamic loading of polycrystalline shape memory alloy rods. *Mech. Mater.* **35**, 689–716 (2003)
9. Niemczura, J., Ravi-Chandar, K.: Dynamics of propagating phase boundaries in NiTi. *J. Mech. Phys. Solids* **54**, 2136–2161 (2006)

10. Abeyaratne, R., Knowles, J.K.: Dynamics of propagating phase boundaries: thermoelastic solids with heat conduction. *Arch. Rational. Mech. Anal.* **126**, 203–230 (1994)
11. Abeyaratne, R., Knowles, J.K.: Dynamics of propagating phase boundaries: adiabatic theory for thermoelastic solids. *Physica D (Nonlinear Phenomena)* **79**, 269–288 (1994)
12. Abeyaratne, R., Knowles, J.K.: Impact-induced phase transitions in thermoelastic solids. *Phil. Trans. R. Soc. Lond. A* **355**, 843–867 (1997)
13. Chen, Y.C., Lagoudas, D.C.: Impact induced phase transformation in shape memory alloys. *J. Mech. Phys. Solids* **48**, 275–300 (2000)
14. Chen, Y.C., Lagoudas, D.C.: Wave propagation in shape memory alloy rods under impulsive loads. *Proc. R. Soc. A* **461**, 3871–3892 (2005)
15. Vainchtein, A.: Dynamics of non-isothermal martensitic phase transitions and hysteresis. *Int. J. Solids Struct.* **39**, 3387–3408 (2002)
16. Vainchtein, A.: Non-isothermal kinetics of a moving phase boundary. *Continuum Mech. Thermodyn.* **15**, 1–19 (2003)
17. Slemrod, M.: Dynamic phase transitions in a van der Waals fluid. *J. Diff. Eqs.* **52**, 1–23 (1984)
18. Abeyaratne, R., Knowles, J.K.: Implications of viscosity and strain gradient effects for kinetics of propagating phase boundaries in solids. *SIAM J. Appl. Math.* **51**, 1205–1221 (1991)
19. Turteltaub, S.: Viscosity and strain gradient effects on the kinetics of propagating phase boundaries in solids. *J. Elast.* **46**, 53–90 (1997)
20. Ngan, S.-C., Truskinovsky, L.: Thermal trapping and kinetics of martensitic phase boundaries. *J. Mech. Phys. Solids* **47**, 141–172 (1999)
21. Ngan, S.-C., Truskinovsky, L.: Thermoelastic aspects of dynamic nucleation. *J. Mech. Phys. Solids* **50**, 1193–1229 (2002)
22. Făciu, C., Mihăilescu-Suliciu, M.: On modelling phase propagation in SMAs by a Maxwellian thermo-viscoelastic approach. *Int. J. Solids Struct.* **39**, 3811–3830 (2002)
23. Dunn, J.E., Fosdick, R.L.: Steady, structured shock waves. Part 1: Thermoelastic materials. *Arch. Rat. Mech. Anal.* **104**, 295–365 (1988)
24. Shaw, J.A.: Simulations of localized thermo-mechanical behavior in a NiTi shape memory alloy. *Int. J. Plast.* **16**, 541–562 (2000)
25. Truskinovsky, L.: About the “normal growth” approximation in the dynamical theory of phase transitions. *Continuum Mech. Thermodyn.* **6**, 185–208 (1994)
26. Abeyaratne, R., Kim, S.-J., Knowles, J.K.: A one-dimensional continuum model for shape memory alloys. *Int. J. Solids Struct.* **31**, 2229–2249 (1994)
27. Shaw, J.A., Kyriakides, S.: On the nucleation and propagation of phase transformation fronts in a NiTi alloy. *Acta Mater.* **45**, 683–700 (1997)
28. Gilbarg, D.: The existence and limit behavior of the one-dimensional shock layer. *Am. J. Math.* **73**, 256–274 (1951)
29. Pego, R.L.: Nonexistence of a shock layer in gas dynamics with a nonconvex equation of state. *Arch. Ration. Mech. Anal.* **94**, 165–178 (1986)
30. Landau, L.D., Lifschitz, E.M.: *Mécanique des fluides*, Collection Physique Théorique, vol. 6, Editions Mir 2eme édn. Moscou (1989)
31. Vainchtein, A., Rosakis, P.: Hysteresis and stick-slip motion of the interfaces in dynamic models of phase transitions. *J. Nonlinear Sci.* **9**, 697–719 (1999)
32. Vainchtein, A.: Stick-slip interface motion as a singular limit of the viscosity-capillarity model. *Math. Mech. Solids* **6**, 323–341 (2001)